

SANDIA REPORT

SAND2001-0527

Unlimited Release

Printed February 2001

Gridless Compressible Flow: A White Paper

James H. Strickland

Prepared by
Sandia National Laboratories
Albuquerque, New Mexico 87185 and Livermore, California 94550

Sandia is a multiprogram laboratory operated by Sandia Corporation,
a Lockheed Martin Company, for the United States Department of
Energy under Contract DE-AC04-94AL85000.

Approved for public release; further dissemination unlimited.



Sandia National Laboratories

Issued by Sandia National Laboratories, operated for the United States Department of Energy by Sandia Corporation.

NOTICE: This report was prepared as an account of work sponsored by an agency of the United States Government. Neither the United States Government, nor any agency thereof, nor any of their employees, nor any of their contractors, subcontractors, or their employees, make any warranty, express or implied, or assume any legal liability or responsibility for the accuracy, completeness, or usefulness of any information, apparatus, product, or process disclosed, or represent that its use would not infringe privately owned rights. Reference herein to any specific commercial product, process, or service by trade name, trademark, manufacturer, or otherwise, does not necessarily constitute or imply its endorsement, recommendation, or favoring by the United States Government, any agency thereof, or any of their contractors or subcontractors. The views and opinions expressed herein do not necessarily state or reflect those of the United States Government, any agency thereof, or any of their contractors.

Printed in the United States of America. This report has been reproduced directly from the best available copy.

Available to DOE and DOE contractors from
U.S. Department of Energy
Office of Scientific and Technical Information
P.O. Box 62
Oak Ridge, TN 37831

Telephone: (865)576-8401
Facsimile: (865)576-5728
E-Mail: reports@adonis.osti.gov
Online ordering: <http://www.doe.gov/bridge>

Available to the public from
U.S. Department of Commerce
National Technical Information Service
5285 Port Royal Rd
Springfield, VA 22161

Telephone: (800)553-6847
Facsimile: (703)605-6900
E-Mail: orders@ntis.fedworld.gov
Online order: <http://www.ntis.gov/ordering.htm>



SAND2001-0527
Unlimited Release
Printed February 2001

Gridless Compressible Flow: A White Paper

James H. Strickland
*Engineering Sciences Center
Sandia National Laboratories
P.O. Box 5800
Albuquerque, New Mexico 87185-0835*

Abstract

In this paper the development of a gridless method to solve compressible flow problems is discussed. The governing evolution equations for velocity divergence δ , vorticity ω , density ρ , and temperature T are obtained from the primitive variable Navier-Stokes equations. Simplifications to the equations resulting from assumptions of ideal gas behavior, adiabatic flow, and/or constant viscosity coefficients are given. A general solution technique is outlined with some discussion regarding alternative approaches. Two radial flow model problems are considered which are solved using both a finite difference method and a compressible particle method. The first of these is an isentropic inviscid 1D spherical flow which initially has a Gaussian temperature distribution with zero velocity everywhere. The second problem is an isentropic inviscid 2D radial flow which has an initial vorticity distribution with constant temperature everywhere. Results from the finite difference and compressible particle calculations are compared in each case. A summary of the results obtained herein is given along with recommendations for continuing the work.

(this page intentionally left blank)

Table of Contents

1	INTRODUCTION	7
1.1	Motivation	7
1.2	Past and Present Efforts	7
1.3	Paper Organization	8
2	GOVERNING EQUATIONS	9
2.1	Governing Equations for Newtonian Fluids	9
2.2	Divergence Evolution Equation	10
2.3	Vorticity Evolution Equation	11
2.4	Simplifications to the Equations	12
3	SOLUTION TECHNIQUES	15
3.1	General Method	15
3.2	Particle Generation at Body Surfaces	15
3.3	Viscous Diffusion	16
3.4	Acoustic Propagation	16
3.5	On the Solution of Evolution Equations	17
3.5.1	Continuity/Energy	17
3.5.2	Vorticity	19
3.5.3	Divergence	20
3.5.4	Moving Least Squares	21
4	MODEL PROBLEMS	23
4.1	1D Spherical Flow: Temperature Disturbance	23
4.1.1	Finite Difference Solution	23
4.1.2	Compressible Particle Solution	26
4.2	2D Radial Flow: Vorticity Disturbance	30
4.2.1	Finite Difference Solution	31
4.2.2	Compressible Particle Solution	34
5	DISCUSSION	39
5.1	General Observations	39
5.2	Some Questions to Answer	39
5.3	A Set of Investigations	40
5.4	Some Model Problems	40
6	REFERENCES	43

(this page intentionally left blank)

1 INTRODUCTION

1.1 Motivation

Sandia National Laboratories has been tasked with the simulation of nuclear weapons parachute performance. These high performance parachutes must operate under a variety of conditions some of which are in the compressible flow regime. At the beginning of the deployment sequence, the parachute is packed in a bag to a density approaching that of oak wood. After the bag is stripped off, the parachute undergoes a very rapid inflation process with large geometry changes. These parachutes are constructed from thousands of ribbon elements which have gaps between them. These gaps typically comprise about 20% of the total area of the parachute. A discussion of the fluid dynamics of parachute inflation and relatively recent simulation attempts are given by Peterson, Strickland, and Higuchi [1] as well as Strickland and Higuchi [2].

As part of the Accelerated Strategic Computing Initiative (ASCI), Sandia has developed a 3D incompressible gridless vortex code (VIPAR) which is capable of simulating unsteady bluff-body flow over time-dependent geometries. In FY2001, Sandia will embark upon a joint exploratory effort with Professor Nitsche at the University of New Mexico who has received funding for a Sandia University Research Proposal (SURP) regarding gridless compressible methods. The level of effort for this initial investigation will be quite modest in light of the tremendous challenges associated with the formulation and implementation of such a method.

In the present paper, the notion of extending classical incompressible gridless vortex methods into the compressible regime is discussed along with possible directions which one might take to eventually obtain a mature algorithm. The general motivation for extending the gridless vortex method is to be able to capitalize upon its inherent advantages (no gridding in the fluid volume, limited computational domains, easily satisfied farfield boundary conditions, etc.).

1.2 Past and Present Efforts

Although there is not a large body of work associated with compressible gridless vortex methods, there are several researchers who have made progress in this area. These efforts have been briefly reviewed by Homicz [3] and Nitsche [4]. In general, the works of Mas-Gallic, Louaked, and Pironneau [5], Mas-Gallic [6], and Sod [7,8] are not truly gridless in that they solve a portion of the problem on a grid, but they do provide some important insights. The works of Ogami and Cheer [9,10] are gridless but require particles to be distributed over the entire fluid flow domain.

Very recently, a 2D vortex method for isentropic compressible flows was presented by Eldridge, Colonius, and Leonard [11]. While details of this work are not yet available, viewgraphs from their presentation indicate that this approach most closely follows our intended direction [3,4] for the development of a 3D algorithm. In general, this method tracks the evolution of the velocity divergence field δ , the vorticity field ω , and the enthalpy field h . Using the Helmholtz decomposition of a vector field, the velocity field is reconstructed at each time step from δ and ω using a fast multipole solver [12,13]. In solving the evolution equations

which contain the Laplacians of vorticity ω and enthalpy h , Eldridge et al. [11] use the particle strength exchange (PSE) method which was originally developed by Degond and Mas-Gallic [14]. Gharakhani [15] suggests that a vorticity redistribution method (VRM) originally developed by Subramaniam [16] may prove superior to the PSE method with regard to reducing the number of elements and rediscrretization requirements associated with the PSE method.

1.3 Paper Organization

In Section 2, the governing evolution equations for δ , ω , ρ , and T are obtained from the primitive variable Navier-Stokes equations. Simplifications to the equations resulting from assumptions of ideal gas behavior, adiabatic flow, and/or constant viscosity coefficients are given. In Section 3, general solution techniques are discussed. Section 4 contains radial flow initial value model problems which are solved using a discrete particle method. The first of these is an isentropic inviscid 1D spherical flow which initially has a Gaussian temperature distribution with zero velocity everywhere. The second problem is an isentropic inviscid 2D radial flow which initially has a vorticity distribution with constant temperature everywhere. The results in each case are compared with those from finite difference simulations. In Section 5 a discussion and summary of the results obtained herein is given along with recommendations for continuing the work.

2 GOVERNING EQUATIONS

2.1 Governing Equations for Newtonian Fluids

The continuity equation is given by:

$$\frac{\partial \rho}{\partial t} + (\mathbf{u} \cdot \nabla) \rho = -\rho(\nabla \cdot \mathbf{u}). \quad (1)$$

The Navier-Stokes momentum equation is given by:

$$\rho \frac{\partial \mathbf{u}}{\partial t} + \rho(\mathbf{u} \cdot \nabla) \mathbf{u} = -\nabla p + \nabla[\lambda(\nabla \cdot \mathbf{u})] + \nabla \cdot [\mu(\nabla \mathbf{u} + \nabla^T \mathbf{u})] + \rho \mathbf{f}. \quad (2)$$

Here, $\nabla \mathbf{u}$ is the deformation rate tensor and $\nabla^T \mathbf{u} \equiv (\nabla \mathbf{u})^T$ is its transpose. As given by Curry [17], the sum of the deformation rate tensor and its transpose is equal to twice the shear rate tensor S_{ij} :

$$\nabla \mathbf{u} + \nabla^T \mathbf{u} = 2S_{ij} = \frac{\partial u_j}{\partial x_i} + \frac{\partial u_i}{\partial x_j}. \quad (3)$$

Of note in Equation 2 is the fact that for compressible flow there is an additional viscous term on the right hand side resulting from non-zero divergence of velocity. For example, use of Stoke's hypothesis for the viscosity coefficients $\left(\lambda = -\frac{2}{3}\mu\right)$ along with an assumption that the viscosity μ is constant, gives rise to the additional viscous term $\frac{1}{3}\nu \nabla(\nabla \cdot \mathbf{u})$ in the following momentum equation:

$$\frac{\partial \mathbf{u}}{\partial t} + (\mathbf{u} \cdot \nabla) \mathbf{u} = -\frac{\nabla p}{\rho} + \frac{1}{3}\nu \nabla(\nabla \cdot \mathbf{u}) + \nu \nabla^2 \mathbf{u} + \mathbf{f}. \quad (4)$$

The energy equation is given by:

$$\rho \frac{\partial e}{\partial t} + \rho(\mathbf{u} \cdot \nabla) e = -p(\nabla \cdot \mathbf{u}) + \nabla \cdot (k \nabla T) + \lambda(\nabla \cdot \mathbf{u})^2 + \mu[\nabla \mathbf{u} : (\nabla \mathbf{u} + \nabla^T \mathbf{u})], \quad (5)$$

where the tensor multiplication notation “:” is from Bird, Stewart, and Lightfoot [18]. The tensor product $a:b$ is defined by $a:b \equiv \sum_i \sum_j a_{ij} b_{ji}$. Thus, $\nabla \mathbf{u} : (\nabla \mathbf{u} + \nabla^T \mathbf{u}) = \frac{\partial u_j}{\partial x_i} (2S_{ji})$.

To complete the set of equations, one must provide equations of state for the pressure $p(\rho, T)$ and energy $e(\rho, T)$ such as $e = C_v T$ and $p = \rho R T$.

2.2 Divergence Evolution Equation

To obtain the divergence evolution equation, Equation 2 is first rewritten as:

$$\frac{\partial \mathbf{u}}{\partial t} = -(\mathbf{u} \cdot \nabla) \mathbf{u} - \frac{\nabla p}{\rho} + \frac{1}{\rho} \Psi(\lambda, \mu, \mathbf{u}) + \mathbf{f}, \quad (6)$$

$$\Psi(\lambda, \mu, \mathbf{u}) \equiv \nabla[\lambda(\nabla \cdot \mathbf{u})] + \nabla \cdot [\mu(\nabla \mathbf{u} + \nabla^T \mathbf{u})].$$

Taking the divergence of Equation 6, denoting the velocity divergence by $\delta \equiv \nabla \cdot \mathbf{u}$, and adding $(\mathbf{u} \cdot \nabla)\delta$ to both sides yields:

$$\frac{\partial \delta}{\partial t} + (\mathbf{u} \cdot \nabla)\delta = (\mathbf{u} \cdot \nabla)\delta - \nabla \cdot [(\mathbf{u} \cdot \nabla) \mathbf{u}] + \nabla \cdot \left(-\frac{\nabla p}{\rho} + \frac{\Psi}{\rho} + \mathbf{f} \right). \quad (7)$$

The first two terms on the right hand side are easily written in index notation as:

$$(\mathbf{u} \cdot \nabla)(\nabla \cdot \mathbf{u}) - \nabla \cdot [(\mathbf{u} \cdot \nabla) \mathbf{u}] = u_j \frac{\partial}{\partial x_j} \left(\frac{\partial u_i}{\partial x_i} \right) - \frac{\partial}{\partial x_i} \left(u_j \frac{\partial u_i}{\partial x_j} \right) = -\frac{\partial u_j \partial u_i}{\partial x_i \partial x_j}, \quad (8)$$

This in turn can be written as:

$$\frac{\partial u_j \partial u_i}{\partial x_i \partial x_j} = \nabla \mathbf{u} : \nabla \mathbf{u} = S_{ij} S_{ij} - \Omega_{ij} \Omega_{ij}, \quad (9)$$

where Ω_{ij} is the rotation rate tensor $\Omega_{ij} \equiv \frac{1}{2} \left(\frac{\partial u_i}{\partial x_j} - \frac{\partial u_j}{\partial x_i} \right)$. Therefore, the divergence evolution equation can be given by:

$$\frac{D\delta}{Dt} = -\nabla \cdot \left(\frac{\nabla p}{\rho} - \frac{\Psi}{\rho} - \mathbf{f} \right) - \nabla \mathbf{u} : \nabla \mathbf{u}. \quad (10)$$

The first two terms on the right hand side of Equation 7 can alternatively be expressed as:

$$(\mathbf{u} \cdot \nabla)\delta - \nabla \cdot [(\mathbf{u} \cdot \nabla) \mathbf{u}] = \nabla \cdot (\mathbf{u}\delta) - \delta^2 - \nabla \cdot \left(\frac{1}{2} \nabla u^2 - \mathbf{u} \times \boldsymbol{\omega} \right), \quad (11)$$

so that the divergence evolution equation is given by:

$$\frac{D\delta}{Dt} = -\nabla \cdot \left(\frac{\nabla p}{\rho} + \frac{1}{2} \nabla u^2 - \mathbf{u} \times \boldsymbol{\omega} - \mathbf{u} \delta - \frac{\Psi}{\rho} - \mathbf{f} \right) - \delta^2. \quad (12)$$

The viscous term can be simplified significantly if it is assumed that the kinematic viscosity ν as well as the dynamic viscosity μ are equal to a constant. Clearly, this assumption is valid only if the change in ρ is small since $\nu = \mu/\rho$. Using the Stoke's hypothesis for the viscosity coefficients $\left(\lambda = -\frac{2}{3}\mu \right)$ then:

$$\frac{\Psi}{\rho} = \frac{1}{3} \nu \nabla^2 \delta + \nu \nabla^2 \mathbf{u}. \quad (13)$$

The divergence of Equation 13 is:

$$\nabla \cdot \left(\frac{\Psi}{\rho} \right) = \frac{1}{3} \nu \nabla^2 \delta + \nu \nabla^2 \delta = \frac{4}{3} \nu \nabla^2 \delta. \quad (14)$$

It should be noted that if only the dynamic viscosity μ is assumed to be equal to a constant then an additional term containing the density gradient appears:

$$\nabla \cdot \left(\frac{\Psi}{\rho} \right) = \frac{4}{3} \nu \nabla^2 \delta - \left(\frac{\nabla \rho}{\rho} \right) \cdot \left(\frac{\Psi}{\rho} \right). \quad (15)$$

2.3 Vorticity Evolution Equation

Taking the curl of Equation 6 and adding $(\mathbf{u} \cdot \nabla)\boldsymbol{\omega}$ to both sides yields:

$$\frac{\partial \boldsymbol{\omega}}{\partial t} + (\mathbf{u} \cdot \nabla)\boldsymbol{\omega} = (\mathbf{u} \cdot \nabla)\boldsymbol{\omega} - \nabla \times [(\mathbf{u} \cdot \nabla)\mathbf{u}] - \nabla \times \left(\frac{\nabla p}{\rho} - \frac{\Psi}{\rho} - \mathbf{f} \right). \quad (16)$$

The term $\nabla \times [(\mathbf{u} \cdot \nabla)\mathbf{u}]$ can be expanded by using the following vector operations:

$$-\nabla \times [(\mathbf{u} \cdot \nabla)\mathbf{u}] = -\nabla \times \left(\frac{1}{2} \nabla u^2 - \mathbf{u} \times \boldsymbol{\omega} \right) = \nabla \times (\mathbf{u} \times \boldsymbol{\omega}), \quad (17)$$

$$\nabla \times (\mathbf{u} \times \boldsymbol{\omega}) = (\boldsymbol{\omega} \cdot \nabla)\mathbf{u} - \boldsymbol{\omega} \delta - (\mathbf{u} \cdot \nabla)\boldsymbol{\omega}.$$

The first two terms on the right hand side of Equation 16 can thus be replaced by:

$$(\mathbf{u} \cdot \nabla)\boldsymbol{\omega} - \nabla \times [(\mathbf{u} \cdot \nabla)\mathbf{u}] = (\boldsymbol{\omega} \cdot \nabla)\mathbf{u} - \boldsymbol{\omega}\delta, \quad (18)$$

so that Equation 16 can be written as:

$$\frac{D\boldsymbol{\omega}}{Dt} = (\boldsymbol{\omega} \cdot \nabla)\mathbf{u} - \boldsymbol{\omega}\delta - \nabla \times \left(\frac{\nabla p}{\rho} - \frac{\Psi}{\rho} - \mathbf{f} \right). \quad (19)$$

The viscous term for constant kinematic viscosity ν and constant dynamic viscosity μ is given by:

$$\nabla \times \left(\frac{\Psi}{\rho} \right) = \nabla \times \left(\frac{1}{3}\nu \nabla \delta + \nu \nabla^2 \mathbf{u} \right) = \nabla \times (\nu \nabla^2 \mathbf{u}) = \nu \nabla^2 \boldsymbol{\omega}. \quad (20)$$

For the case where the dynamic viscosity μ is equal to a constant but not the kinematic viscosity ν , the viscous term in the vorticity equation becomes:

$$\nabla \times \left(\frac{\Psi}{\rho} \right) = \nu \nabla^2 \boldsymbol{\omega} - \left(\frac{\nabla \rho}{\rho} \right) \times \left(\frac{\Psi}{\rho} \right). \quad (21)$$

2.4 Simplifications to the Equations

The evolution equations for density, divergence, vorticity, and internal energy, are repeated here for convenience:

$$\frac{D\rho}{Dt} = -\rho\delta, \quad (22)$$

$$\frac{D\delta}{Dt} = -\nabla \cdot \left(\frac{\nabla p}{\rho} - \frac{\Psi}{\rho} - \mathbf{f} \right) - \nabla \mathbf{u} : \nabla \mathbf{u}, \quad (23)$$

$$\frac{D\boldsymbol{\omega}}{Dt} = (\boldsymbol{\omega} \cdot \nabla)\mathbf{u} - \boldsymbol{\omega}\delta - \nabla \times \left(\frac{\nabla p}{\rho} - \frac{\Psi}{\rho} - \mathbf{f} \right), \quad (24)$$

$$\rho \frac{De}{Dt} = -p\delta + \nabla \cdot (k\nabla T) + \lambda\delta^2 + \mu[\nabla \mathbf{u} : (\nabla \mathbf{u} + \nabla^T \mathbf{u})]. \quad (25)$$

If it is first assumed that there are no body forces and the viscosity coefficients μ and ν are nearly constant (i.e. $\frac{\nabla \rho}{\rho} \ll 1$) and are governed by Stoke's hypothesis then Equations 22-25 become:

$$\frac{D\rho}{Dt} = -\rho\delta, \quad (26)$$

$$\frac{D\delta}{Dt} = -\nabla \cdot \left(\frac{\nabla p}{\rho} \right) - \nabla \mathbf{u} : \nabla \mathbf{u} + \frac{4}{3} \nu \nabla^2 \delta, \quad (27)$$

$$\frac{D\omega}{Dt} = (\omega \cdot \nabla) \mathbf{u} - \omega \delta - \nabla \times \left(\frac{\nabla p}{\rho} \right) + \nu \nabla^2 \omega, \quad (28)$$

$$\frac{De}{Dt} = -\frac{p}{\rho} \delta + \frac{1}{\rho} \nabla \cdot (k \nabla T) - \frac{2}{3} \nu \delta^2 + \nu [\nabla \mathbf{u} : (\nabla \mathbf{u} + \nabla^T \mathbf{u})]. \quad (29)$$

Assuming that $e = C_v T$ and $p = \rho R T$ then the energy equation can be written as:

$$\frac{DT}{Dt} = -(\gamma-1)T\delta + \frac{1}{\rho C_v} \nabla \cdot (k \nabla T) - \frac{2}{3} \frac{\nu}{C_v} \delta^2 + \frac{\nu}{C_v} [\nabla \mathbf{u} : (\nabla \mathbf{u} + \nabla^T \mathbf{u})], \quad (30)$$

where $\gamma \equiv \frac{C_p}{C_v}$ and $R \equiv C_p - C_v$. There are now five equations (Equations 26, 27, 28, 30, and $p = \rho R T$) and five unknowns (p , ρ , T , δ , and ω).

If the conduction heat transfer and viscous terms in the energy equation are also neglected then:

$$\frac{DT}{Dt} = -(\gamma-1)T\delta. \quad (31)$$

Eliminating δ from Equations 26 and 31 and using the equation of state yields the following relationships between T , ρ , and p which are recognized as those for an isentropic process in an ideal gas:

$$\frac{T}{T_1} = \left(\frac{\rho}{\rho_1} \right)^{(\gamma-1)} = \left(\frac{p}{p_1} \right)^{\frac{(\gamma-1)}{\gamma}}. \quad (32)$$

Note that if the conduction heat transfer and viscous terms in the energy equation are not negligible, the process is no longer isentropic.

It is now instructive to write the term $\frac{\nabla p}{\rho}$ as a function of the temperature T using the relationships in Equation 32.

$$\frac{\nabla p}{\rho} = \frac{p_1 \nabla \left[\left(\frac{T}{T_1} \right)^{\frac{\gamma}{\gamma-1}} \right]}{\rho_1 \left(\frac{T}{T_1} \right)^{\frac{1}{\gamma-1}}} = \frac{p_1}{\rho_1 T_1} \left(\frac{\gamma}{\gamma-1} \right) \nabla T = \frac{R\gamma}{\gamma-1} \nabla T = C_p \nabla T \quad (33)$$

For an ideal gas, the enthalpy is a function of temperature alone and can be written as:

$$dh = C_p dT \text{ or } \nabla h = C_p \nabla T. \quad (34)$$

Therefore, the pressure gradient term can be written in terms of the enthalpy gradient.

$$\frac{\nabla p}{\rho} = C_p \nabla T = \nabla h. \quad (35)$$

Thus, the baroclinic term $\nabla \times \left(\frac{\nabla p}{\rho} \right) = \nabla \times \nabla h$ in Equation 28 is identically zero. Therefore, the governing equations for a constant viscosity ideal gas with negligible conduction heat transfer and viscous energy dissipation can be written as:

$$\frac{D\delta}{Dt} = -\nabla^2(C_p T) - \nabla \mathbf{u} : \nabla \mathbf{u} + \frac{4}{3} \nu \nabla^2 \delta, \quad (36)$$

$$\frac{D\omega}{Dt} = (\omega \cdot \nabla) \mathbf{u} - \omega \delta + \nu \nabla^2 \omega, \quad (37)$$

$$\frac{DT}{Dt} = -(\gamma-1)T\delta. \quad (38)$$

There are now three equations and three unknowns (T , δ , and ω). The pressure and density, which have been eliminated from this set of equations, may be obtained after-the-fact from Equation 32 if so required. One may also substitute the enthalpy h for $C_p T$ in Equations 36 and 38 so long as C_p is a constant and $h(T) = 0$ for $T = 0$. It is worth noting again that the flow represented by Equations 36-38 is assumed to have negligible heat transfer and viscous dissipation and is therefore isentropic yet it may be rotational as well as viscous.

3 SOLUTION TECHNIQUES

3.1 General Method

In general, the proposed gridless method tracks the evolution of the velocity divergence field δ , the vorticity field ω , and the thermodynamic properties of the fluid (p, ρ, T). Since the solution using the evolution equations (for example Equations 22-25) requires that one connect the particles, the particle velocity field must be reconstructed from the vorticity and divergence fields. Using the Helmholtz decomposition of a vector field, the velocity field is reconstructed at each time step from δ , ω , and a scalar potential function ϕ according to:

$$\mathbf{u}(\mathbf{r}) = \nabla \times \int_{R_\infty} \omega(\mathbf{r}') K(\mathbf{r}, \mathbf{r}') dR(\mathbf{r}') - \nabla \int_{R_\infty} \delta(\mathbf{r}') K(\mathbf{r}, \mathbf{r}') dR(\mathbf{r}') + \nabla \phi. \quad (39)$$

Here, $K(\mathbf{r}, \mathbf{r}')$ is a Green's function which is given by:

$$K(\mathbf{r}, \mathbf{r}') = \begin{cases} \frac{\ln|\mathbf{r} - \mathbf{r}'|}{2\pi} & \text{for 2D} \\ \frac{1}{4\pi|\mathbf{r} - \mathbf{r}'|} & \text{for 3D} \end{cases} \quad (40)$$

It should be noted that the scalar potential ϕ is zero for bodies moving into otherwise undisturbed fluid. It is also assumed in Equation 39 that the volume integrals include all vortex and divergence sheets associated with any boundaries. An alternative interpretation is to include boundary integrals which explicitly account for the presence of such boundaries. For a detailed discussion concerning this alternative interpretation of the Helmholtz decomposition see Kempka et al. [19].

If the integrals in Equation 39 are discretized into N particles or elements and the velocities at the centers of those N particles are required, a simplistic approach will require $O(N^2)$ operations. There are however, a number of fast multipole methods which can be used to efficiently compute these velocities requiring only $O(N \ln N)$, or even $O(N)$ operations. An overview of such methods is given by Greengard [12] as well as Strickland and Baty [13]. Fast multipole methods for 2D planar flows have been developed by Carrier, Greengard, and Rokhlin [21] (see also Strickland and Baty [22,23]). Axisymmetric fast multipole methods have been developed by Strickland and Amos [20]. Recently an efficient 3D fast multipole method has been developed by Cheng, Greengard, and Rokhlin [24]. The VIPAR code uses a 3D fast multipole method based on work by Strickland, Gritzo, Baty, and Homicz [25] which has been optimized for parallel computing by Homicz and Burns [26].

3.2 Particle Generation at Body Surfaces

In order to gain some insight into the treatment of unsteady compressible flow over a bluff body, let us assume that the body which is initially at rest moves into an otherwise undisturbed fluid. To satisfy the velocity boundary conditions on the body, vortex and possibly

divergence sheets are placed on the boundaries. For example, in the work by Strickland [27] for axisymmetric flow over bluff bodies comprised of thin shells, the normal velocity boundary condition is satisfied by placing a set of discrete vortices to mimic vortex sheets on the shell surface such that the stream function is equal to zero at a set of collocation points. The tangential velocity boundary condition is then satisfied by splitting the resulting vortex sheet into two sheets which are then placed on either side of the shell surface. In the work by Wolfe et al. [28] for two-dimensional flow around tubes, the normal velocity boundary condition is satisfied by first assuming a piecewise linear vortex sheets on the tube surface. The normal velocity boundary condition is then satisfied by using a Galerkin scheme which produces a linear system of equations for the unknown vortex sheet strengths. The tangential boundary condition is again satisfied by splitting the vorticity sheet, resulting in vorticity sheets being placed both inside and outside of the tubes. In the VIPAR code [29], two boundary element methods are available for solving the velocity potential on the surface. The first of these assumes constant potential over each triangular surface element while the second approach, developed by Gharakhani, [30] assumes a piecewise linear potential distribution. In both cases the resulting vortex sheet is smoothed to be piecewise linear and then split to satisfy the tangential boundary condition.

In the case of compressible flow, the discretized surface sheets carry not only values of ω but also values of δ and the thermodynamic properties p , ρ , and T . It should be noted that algorithms to compute appropriate wall values for δ and the thermodynamic properties will have to be formulated. This is perhaps a non-trivial task and will require modification of the boundary element computation if it is found that the flux of δ from the wall into the flow cannot be arbitrarily set equal to zero.

3.3 Viscous Diffusion

The surface elements diffuse into the surrounding fluid using one of several diffusion schemes. The diffusion velocity scheme originally developed by Ogami and Akamatsu [31] and further developed by Strickland, Kempka, and Wolfe [32] is a convenient scheme if a wall layer containing a moving grid is used to simulate the viscous boundary layer near the body surface. If particles are used, the PSE method [14] or the VRM [15,16] are more appropriate. Both the PSE method and the VRM redistribute the vorticity so as to account for the Laplacian $\nabla^2 \omega$ on the right hand side of the vorticity evolution equation. According to Gharakhani, the VRM is more accurate since quadratures involving randomly spaced points are not required. In regions next to the undisturbed fluid, the VRM automatically and judiciously adds new particles in regions which are within one diffusion length scale into the undisturbed fluid. The Laplacian $\nabla^2 \delta$ representing the diffusion of divergence appearing in the divergence evolution equation may be treated in a similar fashion.

3.4 Acoustic Propagation

In general, velocity divergence δ is generated in the flow field by pressure gradients through the term $\nabla \cdot \left(\frac{\nabla p}{\rho} \right)$. Also, non-zero values of the shear rate tensor S_{ij} or rotation rate tensor

Ω_{ij} provide new sources of δ . The divergence field itself produces acoustic pressure disturbances via the energy equation which travel outward in an initially radial fashion from each source. If there are no shock waves in the flow, these disturbances travel at the local sound speed $c = \sqrt{\gamma RT}$ plus the local convection velocity. The acoustic pressure pulses from the disturbed fluid which move into the undisturbed fluid and generate new divergence sources are accounted for by adding new particles within one “acoustic length scale.” This is analogous to the addition of particles at the interface between the disturbed and undisturbed fluid so as to account for the viscous diffusion of vorticity.

While divergence is generated in the flow field due to pressure disturbances, vorticity is not, so long as the flow is isentropic. From Equation 37 it can be seen that the only effect that the divergence field has on vorticity is one of dilation in areas where the vorticity already exists. Thus for the isentropic case, vorticity is only generated at the boundaries although it may be intensified by stretching, weakened by dilation, and redistributed by viscous diffusion elsewhere in the flow.

3.5 On the Solution of Evolution Equations

In this section, the evolution equations represented by Equations 36, 37, and 38 along with Equation 32 are examined in greater detail in order to gain insight into their solution. This set of equations allows the values of δ , ω , p , ρ , and T to be updated at each time step. The vorticity equation (Equation 37) and the continuity/energy equation (Equation 38) are familiar and relatively straightforward while the divergence equation (Equation 36) is the least familiar and the most challenging.

Using a particle approach, a general variable $\zeta(\mathbf{r})$ at position \mathbf{r} can be represented by a series of n particles or elements as:

$$\zeta(\mathbf{r}) = \sum_{i=1}^n \zeta_i(\mathbf{r}_i) f_{\zeta}(\mathbf{r}_i - \mathbf{r}), \quad (41)$$

where $\zeta_i(\mathbf{r}_i)$ is the strength of the i^{th} particle, \mathbf{r}_i is its position, and $f_{\zeta}(\mathbf{r})$ is a basis function.

3.5.1 Continuity/Energy

Applying the particle discretization to the continuity/energy equation (Equation 38), yields:

$$\frac{DT_i(\mathbf{r}_i)}{Dt} = -(\gamma - 1)T_i(\mathbf{r}_i)\delta(\mathbf{r}_i), \quad (42)$$

$$\delta(\mathbf{r}_i) = \sum_{j=1}^n \delta_j(\mathbf{r}_j) f_{\delta}(\mathbf{r}_j - \mathbf{r}_i). \quad (43)$$

If so desired, the value of $T_i(\mathbf{r}_i)$ at time $t + \Delta t$ may be obtained implicitly from Equation 42 as:

$$T_i(\mathbf{r}_i)_{t+\Delta t} = T_i(\mathbf{r}_i)_t e^{-(\gamma-1)\bar{\delta}(\mathbf{r}_i)\Delta t}, \quad (44)$$

$$\bar{\delta}(\mathbf{r}_i) = \frac{1}{\Delta t} \int_t^{t+\Delta t} \delta(\mathbf{r}_i) dt. \quad (45)$$

For the case where the basis function $f_{\delta}(\mathbf{r})$ has compact support and does not overlap more than one-half of that support, $\delta(\mathbf{r}_i)$ may be replaced by $\delta_i(\mathbf{r}_i)$ since $\delta(\mathbf{r}_i) = \delta_i(\mathbf{r}_i)$.

A slightly different approach is to assume that each particle has a fixed mass so that the product of the particle density times the particle volume $\rho_i(\mathbf{r}_i)V_i(\mathbf{r}_i)$ is equal to a constant. Thus:

$$\frac{D\rho_i(\mathbf{r}_i)}{Dt} = -\frac{\rho_i(\mathbf{r}_i)}{V_i(\mathbf{r}_i)} \frac{DV_i(\mathbf{r}_i)}{Dt}. \quad (46)$$

From the continuity equation:

$$\frac{D\rho_i(\mathbf{r}_i)}{Dt} = -\rho_i(\mathbf{r}_i)\delta(\mathbf{r}_i), \quad (47)$$

so that the evolution equation for the particle volume from Equations 46 and 47 is:

$$\frac{DV_i(\mathbf{r}_i)}{Dt} = V_i(\mathbf{r}_i)\delta(\mathbf{r}_i). \quad (48)$$

Thus, the alternative approach is to solve the particle volume evolution equation in place of the continuity/energy equation by using Equation 48 and then obtain the density and/or temperature from:

$$\frac{\rho_i(\mathbf{r}_i)_{t+\Delta t}}{\rho_i(\mathbf{r}_i)_t} = \left(\frac{T_i(\mathbf{r}_i)_{t+\Delta t}}{T_i(\mathbf{r}_i)_t} \right)^{\frac{1}{\gamma-1}} = \frac{V_i(\mathbf{r}_i)_t}{V_i(\mathbf{r}_i)_{t+\Delta t}}. \quad (49)$$

3.5.2 Vorticity

The vorticity equation (Equation 37) evaluated at \mathbf{r}_j is:

$$\frac{D\omega(\mathbf{r}_j)}{Dt} = [\omega(\mathbf{r}_j) \cdot \nabla] \mathbf{u}(\mathbf{r}_j) - \omega(\mathbf{r}_j) \delta(\mathbf{r}_i) + \nu \nabla^2 \omega(\mathbf{r}_j). \quad (50)$$

A general method for solving this equation is to split the contribution to $\frac{D\omega(\mathbf{r}_j)}{Dt}$ into three parts corresponding to the three terms on the right hand side of Equation 50.

$$\frac{D\omega(\mathbf{r}_j)}{Dt} = \left. \frac{D\omega(\mathbf{r}_j)}{Dt} \right|_{\text{stretch}} + \left. \frac{D\omega(\mathbf{r}_j)}{Dt} \right|_{\text{dilate}} + \left. \frac{D\omega(\mathbf{r}_j)}{Dt} \right|_{\text{diffuse}}. \quad (51)$$

After applying the particle transformation (Equation 41) to the dilation equation, one obtains:

$$\left. \frac{D\omega_i(\mathbf{r}_i)}{Dt} \right|_{\text{dilate}} = -\omega_i(\mathbf{r}_i) \delta(\mathbf{r}_i). \quad (52)$$

The dilation of vorticity can be handled in an identical manner to that of the density outlined in Section 3.5.1.

Application of Equation 41 to the diffusion portion of the equation yields the following:

$$\left. \frac{D\omega(\mathbf{r}_j)}{Dt} \right|_{\text{diffuse}} = \left. \frac{D \left(\sum_{i=1}^n \omega_i(\mathbf{r}_i) f_{\omega}(\mathbf{r}_i - \mathbf{r}_j) \right)}{Dt} \right|_{\text{diffuse}} = \nu \sum_{i=1}^n \omega_i(\mathbf{r}_i) \nabla_{r_j}^2 f_{\omega}(\mathbf{r}_i - \mathbf{r}_j). \quad (53)$$

Of note is the fact that the Laplacian $\nabla_{r_j}^2$ operates on the basis function $f_{\omega}(\mathbf{r}_i - \mathbf{r}_j)$ so that the resulting basis functions on the left and right hand sides of the equation are not the same.

This means that one cannot simply equate the i^{th} components in the summations to each other. Instead, Equation 53 can be cast in terms of a set of linear equations with unknown values of $\frac{D\omega_i(\mathbf{r}_i)}{Dt}$:

$$[f_{\omega}(\mathbf{r}_i - \mathbf{r}_j)] \left\{ \frac{D\omega_i(\mathbf{r}_i)}{Dt} \right\} = \{ \nu \nabla^2 \omega(\mathbf{r}_j) \}. \quad (54)$$

This linear set of equations tends to be ill conditioned and is computationally expensive to solve. Marshall and Grant [32] devised an iterative method which assumes that the strengths

of the particles near particle j that are contained in the set $Q(j)$ are nearly the same as that at particle j . In the present case, their method leads to a set of iterative equations given by:

$$\frac{D\omega_j(\mathbf{r}_j)^{(q+1)}}{Dt} \sum_{i \in Q} f_{\omega}(\mathbf{r}_i - \mathbf{r}_j) + \sum_{i \in P} f_{\omega}(\mathbf{r}_i - \mathbf{r}_j) \frac{D\omega_i(\mathbf{r}_i)^{(q)}}{Dt} = \nu \nabla^2 \omega(\mathbf{r}_j). \quad (55)$$

Here, $P(j)$ is the complementary set of particles and q is an iteration index. In establishing the amplitudes of Gaussian basis functions to represent a vorticity field, Marshall and Grant used 8-10 neighboring particles and found that the relative strengths converged to 10^{-6} in about 6-8 iterations.

The particle representation for the stretch equation is:

$$\left. \frac{D\omega_i(\mathbf{r}_i)}{Dt} \right|_{\text{stretch}} = (\omega_i(\mathbf{r}_i) \cdot \nabla) \mathbf{u}(\mathbf{r}_i). \quad (56)$$

A number of methods are currently available for simulating the diffusion and stretching of vorticity. Gharakhani [33] provides a 1997 review of methods to model stretching and diffusion. Since that time, his version of the VRM for treating diffusion has become available [15]. In the present version of VIPAR, the stretch term is satisfied by convecting the two ends of a vortex filament which is embedded in each vorton. The present diffusion algorithm in VIPAR is a modified expanding core method which includes the effect of stretch on core growth. This diffusion method will eventually be replaced by the VRM in VIPAR. Work is presently underway on a Sandia contract with Applied Scientific Research (ASR) to obtain improved methods for simulating the vorticity stretching phenomenon.

3.5.3 Divergence

The divergence equation (Equation 36) evaluated at \mathbf{r}_i is:

$$\frac{D\delta(\mathbf{r}_i)}{Dt} = -C_p \nabla^2 T(\mathbf{r}_i) - \nabla \mathbf{u} : \nabla \mathbf{u} + \frac{4}{3} \nu \nabla^2 \delta(\mathbf{r}_i). \quad (57)$$

The viscous diffusion term in the δ evolution equation can be handled in an analogous way to that of the viscous diffusion term in the ω evolution equation. It is interesting to note that δ diffuses at a faster rate than ω . This implies that a particle of a given size cannot have a single basis function for both ω and δ .

The source term $C_p \nabla^2 T$ was treated by Eldridge et al. [11] using the PSE method. It can be noted that this term plays a key role in the wave like behavior associated with disturbances in the flow. One can, for example, obtain the simple linearized wave equation for the temperature by setting all of the convective and viscous terms to zero in Equations 36 and 38 to obtain:

$$\frac{\partial \delta}{\partial t} = -C_p \nabla^2 T, \quad (58)$$

$$\frac{\partial T}{\partial t} = -(\gamma - 1) T \delta. \quad (59)$$

Eliminating δ and neglecting gradients in the local acoustic velocity c yields the wave equation:

$$\frac{\partial^2 T}{\partial t^2} = c^2 \nabla^2 T. \quad (60)$$

This suggests that a time splitting scheme might be devised in which those parts of the divergence and energy equations represented by Equations 58 and 59 are satisfied by the wave equation. For example, fluid particles might first be convected to new positions and then be allowed to behave as wavelike disturbances in the flow. Lighthill [34] and Whitham [35] show that the superposition of such waves is appropriate under certain conditions. A large body of work is available for studying wave phenomenon spanning the range from weak acoustic waves to those produced by nuclear explosions (see Sedov [36]).

The term $-\nabla \mathbf{u} : \nabla \mathbf{u}$ in Equation 36 can take on a variety of forms, several of which are given in the following list:

$$-\nabla \mathbf{u} : \nabla \mathbf{u} = \left\{ \begin{array}{l} \frac{\partial u_j \partial u_i}{\partial x_i \partial x_j} \\ \omega^2 - \nabla \mathbf{u} : \nabla^T \mathbf{u} \\ \Omega_{ij} \Omega_{ij} - S_{ij} S_{ij} \\ -\nabla \cdot \left(\frac{1}{2} \nabla u^2 - \mathbf{u} \times \boldsymbol{\omega} - \mathbf{u} \delta \right) - \delta^2 \\ \mathbf{u} \cdot \nabla \delta - \nabla \cdot [(\mathbf{u} \cdot \nabla) \mathbf{u}] \end{array} \right. . \quad (61)$$

The forms using index notation are, of course, only appropriate for Cartesian coordinates but appear to be relatively simple to compute since they only involve gradients of the velocity vector. On the other hand, the most complicated variation in the list (the 4th item in the list) might be advantageous since it results in a divergence equation whose right hand side is the divergence of a vector plus a simple dilation term:

$$\frac{D\delta}{Dt} = -\nabla \cdot \left[\nabla \left(C_p T + \frac{1}{2} u^2 - \frac{4}{3} v \delta \right) - \mathbf{u} \times \boldsymbol{\omega} - \mathbf{u} \delta \right] - \delta^2. \quad (62)$$

3.5.4 Moving Least Squares

One general method to compute the right hand side of the evolution equations is to use moving least squares (MLS). One might also simply differentiate the basis function in Equation 41. This becomes quite inaccurate, however, when obtaining the Laplacian. Marshall and Grant [37] point out that the MLS method also yields much better results than a centered dif-

ference scheme when obtaining derivatives on an irregular grid. Gossler (see Marshall et al. [38]) provides some error estimates for a quadratic MLS scheme used to compute the Laplacian of the vorticity in a columnar vortex. He concludes that the method is between first- and second-order accurate.

To summarize the MLS method, a variable $\zeta(\mathbf{r}_i)$ in the vicinity of a particle at \mathbf{r}_j is approximated by an N^{th} order Taylor series as:

$$\zeta(\mathbf{r}_i) = \sum_{n=0}^N \frac{1}{n!} \{[(\mathbf{r}_i - \mathbf{r}_j) \cdot \nabla]^n \zeta(\mathbf{r}_j)\}. \quad (63)$$

Assuming that $\zeta(\mathbf{r}_i)$ is known at a set of particles neighboring the particle at \mathbf{r}_j , Equation 63 can be written as a set of linear equations containing the $\frac{1}{6}(N+1)(N+2)(N+3)$ unknown

partial derivatives $\frac{\partial^{i+j+k} \zeta(\mathbf{r}_j)}{\partial x^i \partial y^j \partial z^k}$. In most cases it is desirable, from the standpoint of

smoothness, to include more neighbors than the number of unknown partial derivatives. The resulting overdetermined set of equations is then solved in a least squares sense. Baty (see Wolfe et al. [40]) suggests that a singular value decomposition (SVD) scheme should be used to solve the resulting set of equations. According to Baty, “the least squares solution is the best approximation... in the sense that it minimizes the error in terms of the Euclidean norm.”

Wolfe et al. [40] showed that the arrangement of neighboring particles affects the accuracy of the MLS method. For instance, a set of particles arranged along a line should not be expected to give any information on derivatives perpendicular to that line. Wolfe et al. also investigated the accuracy with which one could obtain $f''(x, y)$ where $f(x, y) = x^4 y^4$ using different neighboring point locations and different orders N for the Taylor series. A third order Taylor series yielded about two orders of magnitude decrease in the error from that of a second order series while a fourth order series reduced the error by about another factor of two.

4 MODEL PROBLEMS

4.1 1D Spherical Flow: Temperature Disturbance

In order to develop some insight into the use of the proposed compressible particle method, consider a purely radial inviscid isentropic flow which has an initial Gaussian temperature distribution given by:

$$\frac{T(r, 0)}{T_\infty} = 1 + \left[\frac{T(0, 0)}{T_\infty} - 1 \right] e^{-\left(\frac{r}{\sigma}\right)^2}. \quad (64)$$

Here, the temperature at time t and radial position r is $T(r, t)$ and $T_\infty \equiv T(\infty, 0)$. The initial radial velocity is zero everywhere.

4.1.1 Finite Difference Solution

First, this initial value problem is solved by using a finite difference solution to the following radial momentum and energy equations which may be obtained from Equations 36 and 38 respectively:

$$\frac{\partial U_r}{\partial t} = -C_p \frac{\partial T}{\partial r} - U_r \frac{\partial U_r}{\partial r}, \quad (65)$$

$$\frac{\partial T}{\partial t} = -U_r \frac{\partial T}{\partial r} - (\gamma - 1) T \left[\frac{\partial U_r}{\partial r} + (n - 1) \frac{U_r}{r} \right], \quad (66)$$

where n is the dimensionality of the problem (1, 2, or 3). Non-dimensional versions of these equations are given by:

$$\frac{\partial U_r^*}{\partial t^*} = -\left(\frac{1}{\gamma - 1}\right) \frac{\partial T^*}{\partial r^*} - U_r^* \frac{\partial U_r^*}{\partial r^*}, \quad (67)$$

$$\frac{\partial T^*}{\partial t^*} = -U_r^* \frac{\partial T^*}{\partial r^*} - (\gamma - 1) T^* \left[\frac{\partial U_r^*}{\partial r^*} + (n - 1) \frac{U_r^*}{r^*} \right], \quad (68)$$

$$r^* = \frac{r}{\sigma}, \quad t^* = \frac{t \sqrt{\gamma R T_\infty}}{\sigma}, \quad U_r^* = \frac{U_r}{\sqrt{\gamma R T_\infty}}, \quad T^* = \frac{T}{T_\infty}, \quad \delta^* = \frac{\delta \sigma}{\sqrt{\gamma R T_\infty}}. \quad (69)$$

The finite difference method used consists of a simple central difference in space and forward difference in time. Time steps of $\Delta t^* = 0.001$ and spatial steps of $\Delta r^* = 0.05$ were used for all of the calculations. While these step sizes appear to give reasonable results, it is suggested that the choice of step sizes as well as the differencing scheme itself be studied in a more rigorous fashion in a follow up investigation.

In Figure 1, the temperature distribution for a 3D radial flow with $\gamma = 1.4$ and $T(0, 0) = 2.0$ is given. As can be seen from this figure, the initially gaussian temperature disturbance does not expand into the surrounding fluid in any sort of self similar way but in fact produces compression waves at its periphery with expansion near the center. As Sedov [36] notes, a similarity solution will exist only for the case where an initial disturbance at $r = 0$ moves into a vacuum.

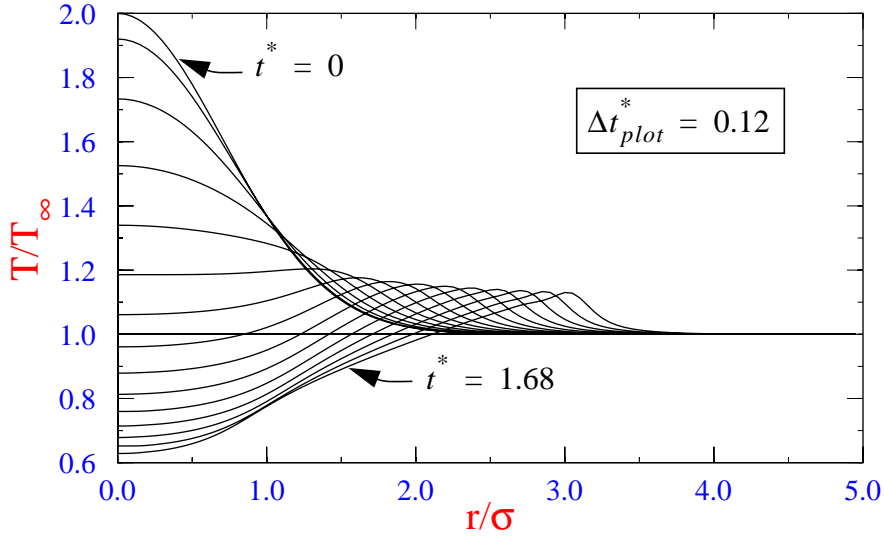


Figure 1. Temperature Distribution for 1D Spherical Flow

The radial velocity distribution is shown in Figure 2. In this figure, the convection velocity initially increases with time in the region $r/\sigma = 1.0$ to a Mach number of about 0.7. As the peripheral waves develop, the peak convective velocity tends to follow the wave crests at a Mach number of about 0.35 near $r/\sigma = 3.0$. Thus an estimate of the wave speed U_W is about 1.35 times the acoustic velocity $\sqrt{\gamma RT_\infty}$ of the undisturbed fluid. It is interesting to note from Figure 1 that the peripheral waves near $r/\sigma = 3.0$ move a distance of about $\Delta r/\sigma = 1/6$ during a time period $\Delta t \sqrt{\gamma RT_\infty}/\sigma = 0.12$ which indicates a wave speed of about 1.39 times the acoustic velocity of the undisturbed fluid.

Another less accurate estimate of the wave speed is to treat the wave as a weak shock wave. The speed of a shock wave into still fluid is given by Anderson [41] as:

$$\frac{U_W}{\sqrt{\gamma RT_\infty}} = \sqrt{\frac{\gamma+1}{2\gamma} \left(\frac{p_2}{p_\infty} - 1 \right) + 1}, \quad (70)$$

where p_2 is the pressure behind the shock. Estimating the pressure p_2 as the pressure at the wave crest and using the isentropic relationship between temperature and pressure with $T_2/T_\infty = 1.14$ from Figure 1, the calculated wave speed is 1.22 times the acoustic velocity of the undisturbed fluid. Such wave speed estimates will eventually be important with regard to inserting new particles at the edges of dilation zones.

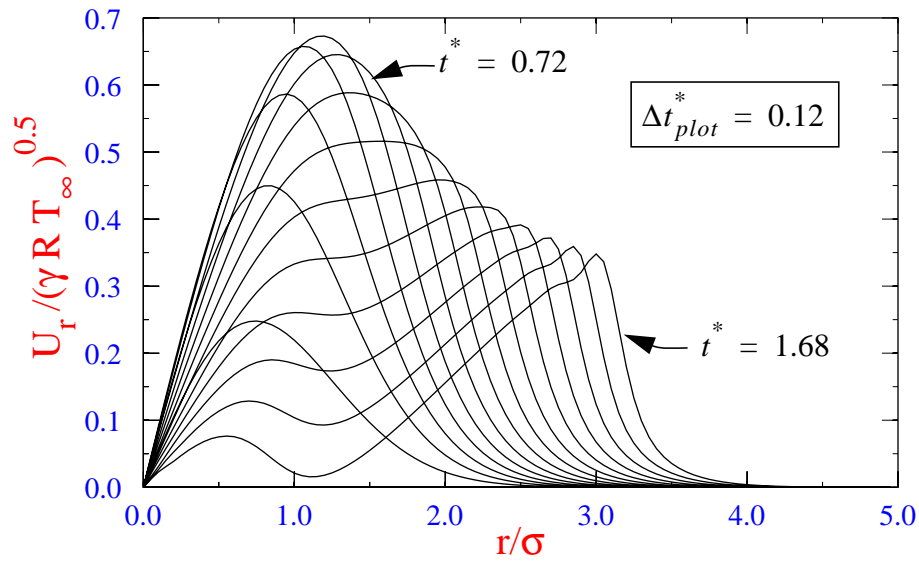


Figure 2. Velocity Distribution for 1D Spherical Flow

In Figure 3, the divergence (computed from the finite difference approximation) of the velocity field is shown. The negative divergence at the periphery essentially cancels out the influence of divergence inside the expanding radial flow at radial positions exterior to the peripheral waves. The radial thickness of this negative divergence region can be seen to be decreasing as the wave moves out. One would expect this thickness to continue to decrease until a shock is formed. Numerical instabilities in the solution are noticeable at the last couple of times which have been plotted.

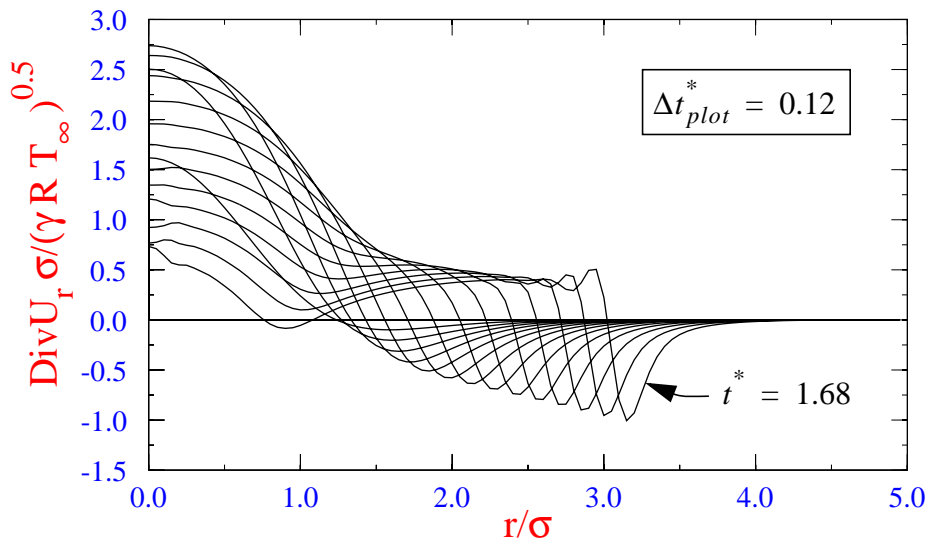


Figure 3. Divergence Distribution for 1D Spherical Flow

4.1.2 Compressible Particle Solution

From Equations 36 and 38 the equations for the evolution of the divergence and temperature fields associated with this problem are:

$$\frac{D\delta}{Dt} = -C_p \nabla^2 T - \nabla \mathbf{u} : \nabla \mathbf{u}, \quad (71)$$

$$\frac{DT}{Dt} = -(\gamma-1)T\delta, \quad (72)$$

where

$$\nabla^2 T = \frac{\partial^2 T}{\partial r^2} + \frac{(n-1)}{r} \frac{\partial T}{\partial r}, \quad (73)$$

$$\nabla \mathbf{u} : \nabla \mathbf{u} = -(\mathbf{u} \cdot \nabla)(\nabla \cdot \mathbf{u}) + \nabla \cdot [(\mathbf{u} \cdot \nabla)\mathbf{u}] = \left(\frac{\partial U_r}{\partial r}\right)^2 + (n-1)\left(\frac{U_r}{r}\right)^2. \quad (74)$$

For the present simulation, a number of discrete particles are placed along the radius. These particles moving at a velocity U_r carry the variables δ and T . The spacial derivatives of T in Equation 73 are calculated using the particle at j and its near neighbors at $j-1$ and $j+1$.

$$\left. \frac{\partial T}{\partial r} \right|_j = w_1 \left. \frac{\partial T}{\partial r} \right|_{j+\frac{1}{2}} + w_2 \left. \frac{\partial T}{\partial r} \right|_{j-\frac{1}{2}}, \quad (75)$$

$$w_1 \equiv \frac{r_j - r_{j-1}}{r_{j+1} - r_{j-1}}, \quad w_2 \equiv \frac{r_{j+1} - r_j}{r_{j+1} - r_{j-1}}, \quad (76)$$

$$\left. \frac{\partial T}{\partial r} \right|_{j-\frac{1}{2}} = \frac{T_j - T_{j-1}}{r_j - r_{j-1}}, \quad \left. \frac{\partial T}{\partial r} \right|_{j+\frac{1}{2}} = \frac{T_{j+1} - T_j}{r_{j+1} - r_j}, \quad (77)$$

$$\left. \frac{\partial^2 T}{\partial r^2} \right|_j = \frac{2}{r_{j+1} - r_{j-1}} \left(\left. \frac{\partial T}{\partial r} \right|_{j+\frac{1}{2}} - \left. \frac{\partial T}{\partial r} \right|_{j-\frac{1}{2}} \right). \quad (78)$$

At $r = 0$ ($j = 1$) these derivatives are:

$$\left. \frac{\partial T}{\partial r} \right|_{j=1} = 0, \quad (79)$$

$$\left. \frac{\partial^2 T}{\partial r^2} \right|_{j=1} = \frac{2}{r_2^2}(T_2 - T_1). \quad (80)$$

Normally, the velocity U_r would be calculated from the scalar potential associated with the divergence δ . However, in the present case since the velocity at $r = 0$ is known, the velocity and velocity gradient can be computed in terms of δ by use of the following development:

$$\delta(r) \equiv \nabla \cdot U_r = \frac{1}{r^{(n-1)}} \frac{\partial}{\partial r} (r^{(n-1)} U_r) = \frac{(n-1)}{r} U_r + \frac{\partial U_r}{\partial r}. \quad (81)$$

Therefore,

$$U_r = r^{-(n-1)} \int_0^r r^{(n-1)} \delta(r) dr, \quad (82)$$

$$\frac{\partial U_r}{\partial r} = \delta(r) - \frac{(n-1)}{r} U_r. \quad (83)$$

Equation 82 can be approximated by:

$$U_r(r_j) \approx \frac{1}{r_j^{(n-1)}} \sum_{i=2}^j \left(\frac{r_i + r_{i-1}}{2} \right)^{(n-1)} \left(\frac{\delta(r_i) + \delta(r_{i-1})}{2} \right) (r_i - r_{i-1}), \quad (84)$$

which can be written in the following recursive form:

$$U_r(r_j) = \left(\frac{r_{j-1}}{r_j} \right) U_r(r_{j-1}) + \frac{1}{2^n} \left(1 + \frac{r_{j-1}}{r_j} \right)^{(n-1)} [\delta(r_j) + \delta(r_{j-1})] (r_j - r_{j-1}). \quad (85)$$

Note: that for $j = 1$ and $r = 0$ that $U_r = 0$ and $\frac{\partial U_r}{\partial r} = 0$.

A summary of the solution method is as follows:

1. Assign zero values to all $\delta(r_j)$ and $U_r(r_j)$.
2. Assign initial values of $T(r_j)$ to all particles using Equation 64.
3. Compute the value of $\frac{D\delta(r_j)}{Dt}$ from Equation 71.
4. Compute the value of $\frac{T(r_j)}{Dt}$ from Equation 72.
5. Update all values of $\delta(r_j)$ and $T(r_j)$.
6. Compute $U_r(r_j)$ from Equation 84.
7. Convect all particles.
8. Go to step 3 and repeat.

Comparisons of the results obtained for the particle simulation versus those for the finite difference calculations are shown in Figures 4-6 using the same time steps and initial spatial discretization. As can be seen for Figure 4, the temperature results are almost indistinguishable between the two computational methods. The particle method yields a slightly steeper wave front for the wave near $r/\sigma = 3.0$. In Figure 5, the velocity results show some noticeable differences at the crests of the last two waves with the particle method yielding more continuous, less oscillatory results. In Figure 6, the divergence results near $r/\sigma = 3.0$ are significantly different with the particle method predicting more spiked results for the negative divergence at the edge of the disturbance. It is proposed that these differences be explained and resolved in follow up studies.

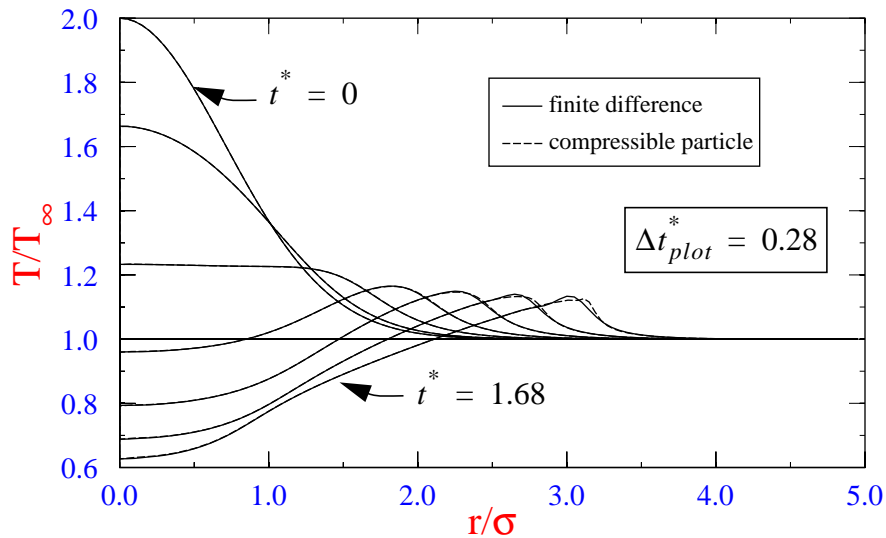


Figure 4. Temperature Comparison for 1D Spherical Flow

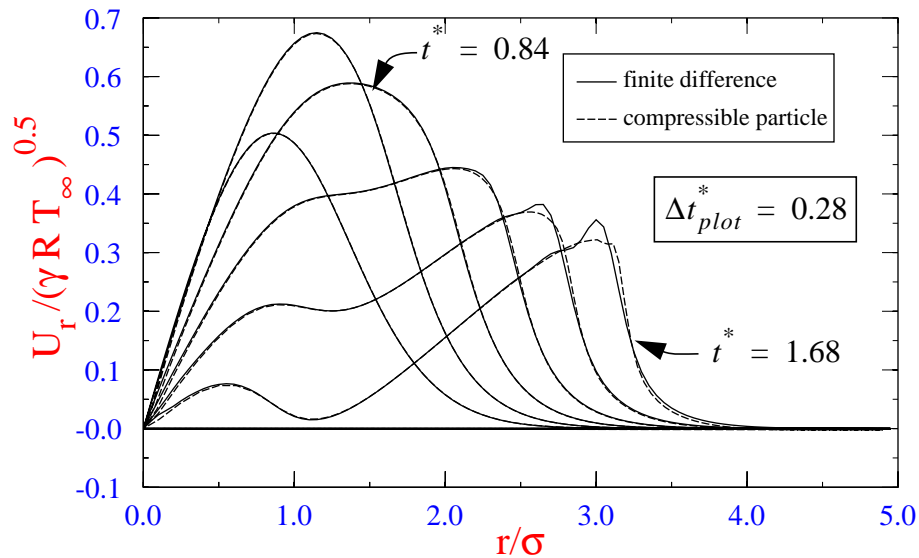


Figure 5. Velocity Comparison for 1D Spherical Flow

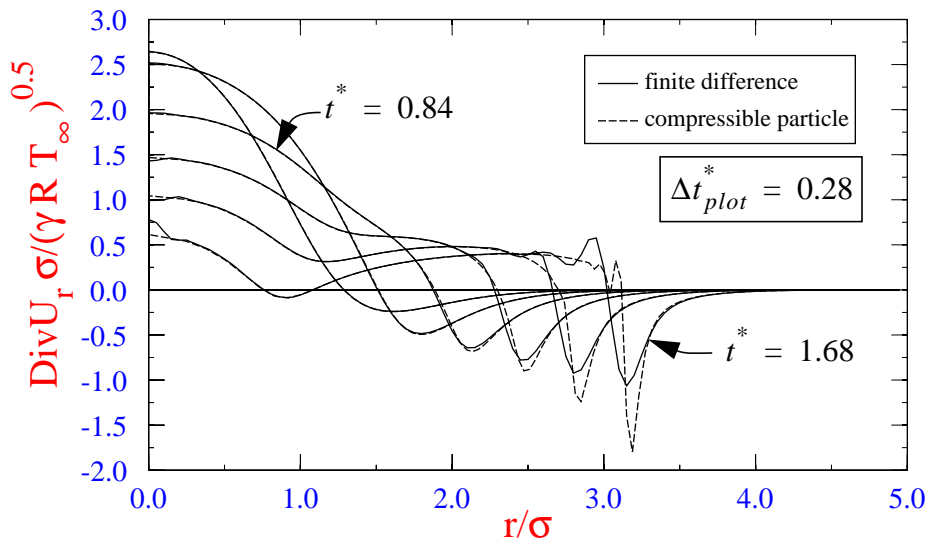


Figure 6. Divergence Comparison for 1D Spherical Flow

In Figure 7, the distribution of particles for the seven time steps displayed in Figures 4-6 is shown. The clustering of particles near $r/\sigma = 3.0$ at the last time step is evident as is the rarefaction of particle densities near the center of the flow. The sharper divergence gradients seen in Figure 6 near $r/\sigma = 3.0$ for the particle simulation may be related to the clustering of particles near this almost shock like feature. Thus, it appears that the particle method possesses a naturally occurring adaptability which is quite advantageous.

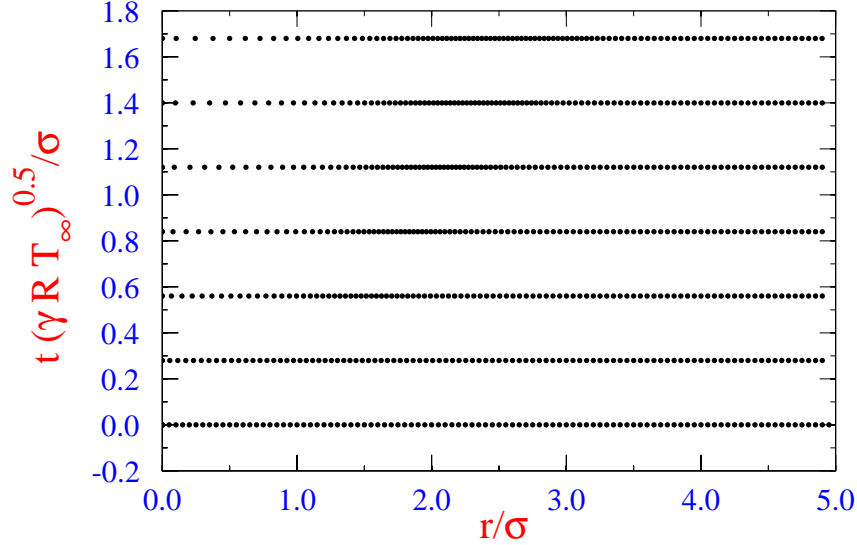


Figure 7. Compressible Particle Distribution

4.2 2D Radial Flow: Vorticity Disturbance

In order to develop some additional insight into the use of the proposed compressible particle method, consider a 2D isentropic swirling flow which is inviscid and which has an initial tangential velocity distribution given by:

$$U_\theta(r, 0) = \sqrt{\gamma R T_\infty} \left(\frac{r}{\sigma}\right)^2 e^{-b\left(\frac{r}{\sigma} - \frac{r_c}{\sigma}\right)^2}, \quad (86)$$

where r_c/σ and b are constants. In non-dimensional terms, Equation 86 becomes:

$$U_\theta^*(r^*, 0) = r^{*2} e^{-b(r^* - r_c^*)^2}. \quad (87)$$

The corresponding initial vorticity distribution is:

$$\omega(r, 0) = \frac{1}{r} \frac{\partial}{\partial r} [r U_\theta(r, 0)] = \frac{r}{\sigma} \left[3 - 2b \frac{r}{\sigma} \left(\frac{r}{\sigma} - \frac{r_c}{\sigma} \right) \right] \frac{\sqrt{\gamma R T_\infty}}{\sigma} e^{-b\left(\frac{r}{\sigma} - \frac{r_c}{\sigma}\right)^2}, \quad (88)$$

$$\omega^*(r^*, 0) = r^* \left[3 - 2b r^* (r^* - r_c^*) \right] e^{-b(r^* - r_c^*)^2} = \left[\frac{3}{r^*} - 2b(r^* - r_c^*) \right] U_\theta^*(r^*, 0). \quad (89)$$

The initial radial velocity is zero everywhere and the temperature $T(r, 0) = T_\infty$.

4.2.1 Finite Difference Solution

The radial momentum, tangential momentum, and energy equations for this problem are given by:

$$\frac{\partial U_r}{\partial t} = -C_p \frac{\partial T}{\partial r} - U_r \frac{\partial U_r}{\partial r} + \frac{U_\theta^2}{r}, \quad (90)$$

$$\frac{\partial U_\theta}{\partial t} = -U_r \left(\frac{\partial U_\theta}{\partial r} + \frac{U_\theta}{r} \right), \quad (91)$$

$$\frac{\partial T}{\partial t} = -U_r \frac{\partial T}{\partial r} - (\gamma - 1) T \left(\frac{\partial U_r}{\partial r} + \frac{U_r}{r} \right). \quad (92)$$

Non-dimensional versions are:

$$\frac{\partial U_r^*}{\partial t^*} = -\left(\frac{1}{\gamma - 1} \right) \frac{\partial T^*}{\partial r^*} - U_r^* \frac{\partial U_r^*}{\partial r^*} + \frac{U_\theta^{*2}}{r^*}, \quad (93)$$

$$\frac{\partial U_\theta^*}{\partial t^*} = -U_r^* \left(\frac{\partial U_\theta^*}{\partial r^*} + \frac{U_\theta^*}{r^*} \right), \quad (94)$$

$$\frac{\partial T^*}{\partial t^*} = -U_r^* \frac{\partial T^*}{\partial r^*} - (\gamma - 1) T^* \left(\frac{\partial U_r^*}{\partial r^*} + \frac{U_r^*}{r^*} \right). \quad (95)$$

The same finite difference scheme as that used for the 1D spherical flow of Section 4.1 was also employed for the present case. The spatial and temporal discretization is also identical ($\Delta t^* = 0.001$, $\Delta r^* = 0.05$). In Figure 8, the vorticity evolution for a 2D swirling flow with $\gamma = 1.4$, $r_c^* = 3/4$, and $b = 4$ is given. Both the vorticity distribution and the tangential velocity distribution shown in Figure 9 are relatively stationary even though the tangential velocity has a maximum in the 0.7-0.8 Mach number range. This is consistent with a statement made by Lighthill [34] about the relative insensitivity of the vorticity field to compressibility effects and to the observations made in Section 3.4 concerning the propagation of δ but not ω at acoustic speeds through the flow.

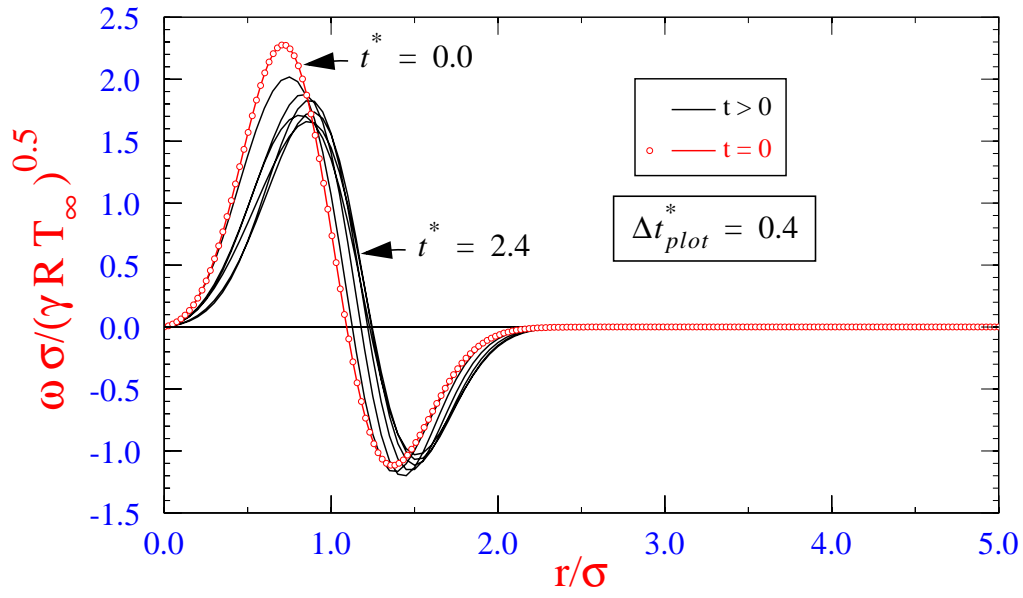


Figure 8. Vorticity Evolution for 2D Radial Flow

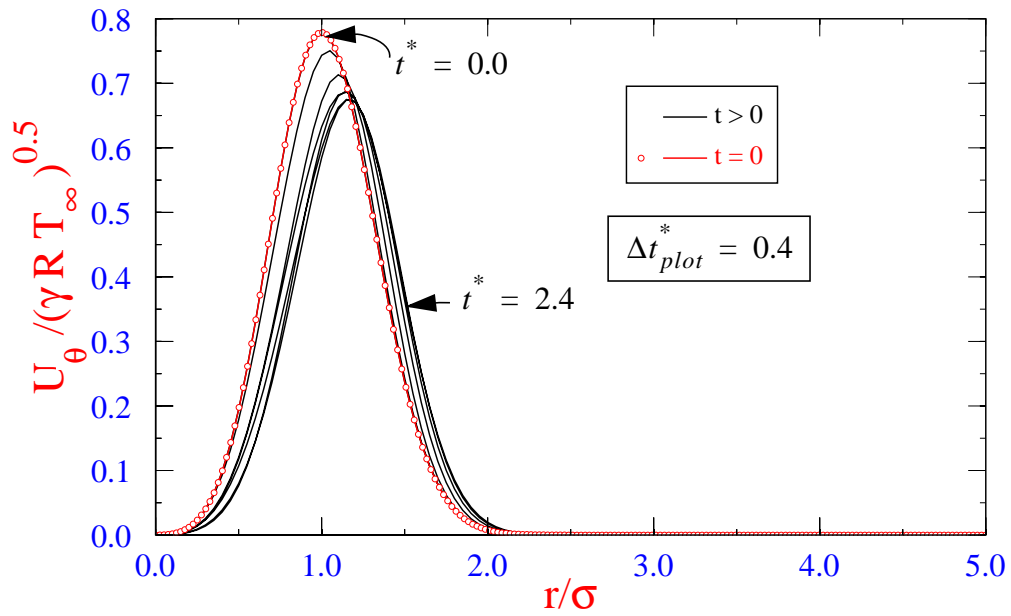


Figure 9. Tangential Velocity Evolution for 2D Radial Flow

The radial temperature distribution is shown in Figure 10. As can be seen from this figure, the peripheral waves move about $0.43r/\sigma$ during the last time step indicating a wave speed of about 1.08 times the acoustic velocity. From Figure 11, the radial fluid velocity at the peak of this peripheral wave is about 0.082 times the acoustic velocity. This also indicates a wave speed of about 1.08 times the acoustic velocity.

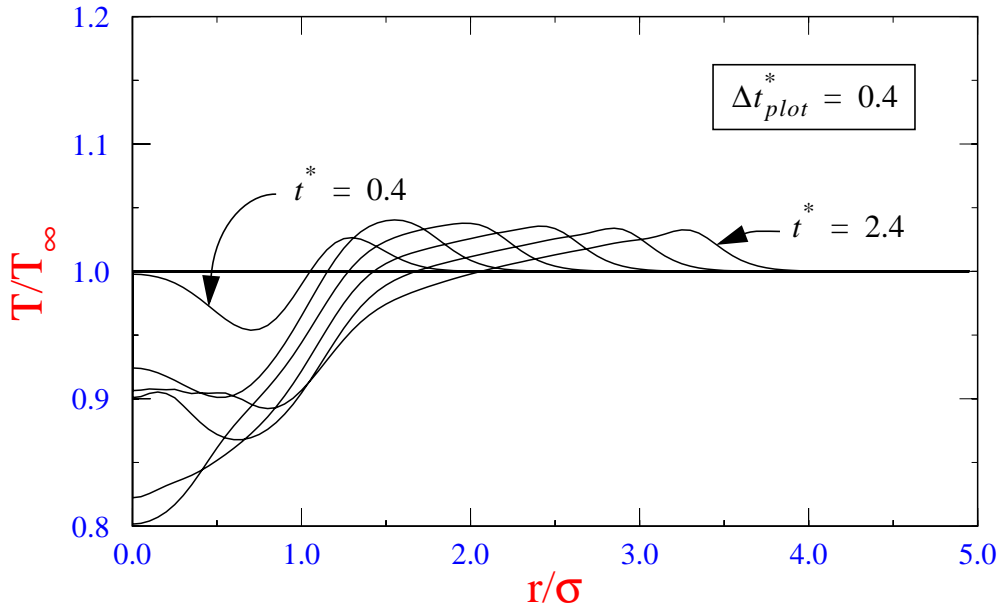


Figure 10. Temperature Evolution for 2D Radial Flow

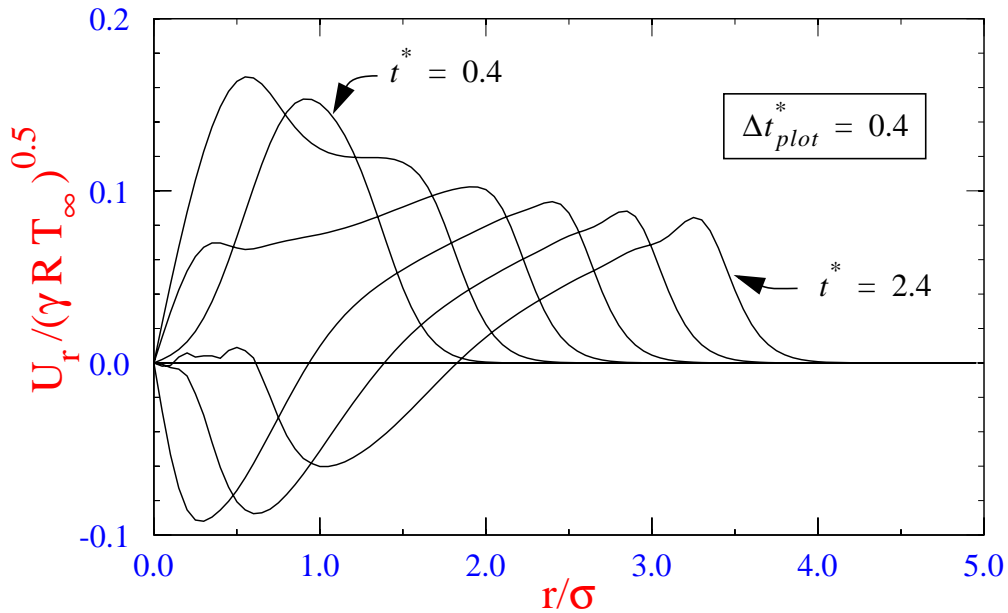


Figure 11. Radial Velocity Evolution for 2D Radial Flow

The divergence of the velocity field is shown in Figure 12 which also shows the peripheral waves traveling into the undisturbed fluid at a speed of about 1.08 times the acoustic velocity. The initial divergence is zero since the initial radial velocity is zero. However, by the second time at which results are plotted, the divergence grows into an “N wave.” The results near the origin are somewhat complex, with the divergence going from zero to positive to negative and back to zero.

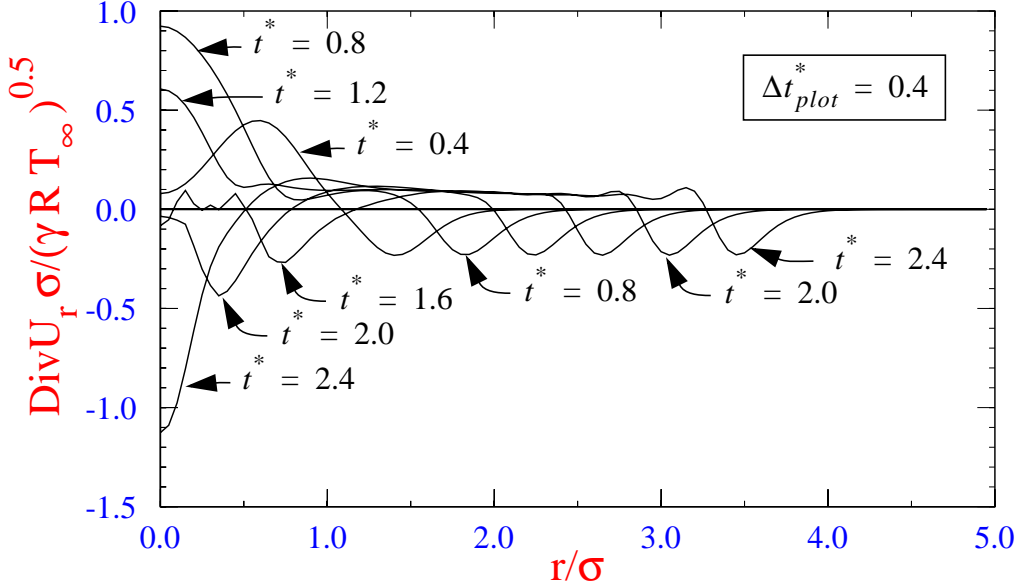


Figure 12. Divergence Evolution for 2D Radial Flow

4.2.2 Compressible Particle Solution

From Equations 36, 37, and 38 the equations for the evolution of the divergence, the vorticity, and the temperature for a 2D inviscid flow are:

$$\frac{D\delta}{Dt} = -\nabla^2(C_p T) - \nabla \mathbf{u} : \nabla \mathbf{u}, \quad (96)$$

$$\frac{D\omega}{Dt} = -\omega\delta, \quad (97)$$

$$\frac{DT}{Dt} = -(\gamma-1)T\delta. \quad (98)$$

where

$$\nabla^2 T = \frac{\partial^2 T}{\partial r^2} + \frac{1}{r} \frac{\partial T}{\partial r}, \quad (99)$$

$$\nabla \mathbf{u} : \nabla \mathbf{u} = -(\mathbf{u} \cdot \nabla)(\nabla \cdot \mathbf{u}) + \nabla \cdot [(\mathbf{u} \cdot \nabla)\mathbf{u}] = \left(\frac{\partial U_r}{\partial r}\right)^2 + \left(\frac{U_r}{r}\right)^2 - \frac{1}{r} \frac{\partial U_\theta^2}{\partial r}. \quad (100)$$

Here, the initial values throughout the domain for δ and T are zero and T_∞ respectively.

Normally, the velocity U_θ would be calculated from the vector potential associated with the vorticity ω . However, in the present case since the velocity at $r = 0$ is known, the velocity and velocity gradient can be computed in terms of ω by use of the following development:

$$\omega(r) \equiv \nabla \times (U_r \hat{e}_r + U_\theta \hat{e}_\theta) = \frac{1}{r} \frac{\partial}{\partial r} (r U_\theta) \hat{e}_z = \left(\frac{U_\theta}{r} + \frac{\partial U_\theta}{\partial r} \right) \hat{e}_z. \quad (101)$$

Therefore,

$$U_\theta = \frac{1}{r} \int_0^r r \omega(r) dr, \quad (102)$$

$$\frac{\partial U_\theta}{\partial r} = \omega(r) - \frac{U_\theta}{r}. \quad (103)$$

Equation 102 can be approximated by:

$$U_\theta(r_j) \approx \frac{1}{r_j} \sum_{i=2}^j \left(\frac{r_i + r_{i-1}}{2} \right) \left(\frac{\omega(r_i) + \omega(r_{i-1})}{2} \right) (r_i - r_{i-1}), \quad (104)$$

which can be written in the following recursive form:

$$U_\theta(r_j) = \left(\frac{r_{j-1}}{r_j} \right) U_\theta(r_{j-1}) + \frac{1}{4} \left(1 + \frac{r_{j-1}}{r_j} \right) [\omega(r_j) + \omega(r_{j-1})] (r_j - r_{j-1}). \quad (105)$$

Comparisons of the results obtained for the particle simulation versus those for the finite difference calculations are shown in Figures 13-17 using the same time steps and initial spatial discretization. As can be seen for Figures 13 and 14 the vorticity and tangential velocity results are virtually indistinguishable between the two computational methods. In Figure 15, the temperature results are almost the same for the two computations although there are some slight differences near the origin and near the periphery. In Figure 16, the differences are noticeable for the radial velocity computation near the origin and near the periphery. In general, the particle method appears to yield more continuous, less oscillatory results. In Figure 17, the divergence results near $r/\sigma = 3.0$ are significantly different with the particle method predicting more spiked results for the negative divergence at the edge of the disturbance. The particle method, on the other hand, is considerably smoother near the origin at the last time step.

Some of the differences near the origin stem from treatment of the governing equations at

$r = 0$. Terms such as $\frac{U_r}{r}$ and $\frac{1}{r} \frac{\partial T}{\partial r}$ are indeterminate at the origin and require either assumptions about their functional form in that region or avoidance of their use altogether. In the work presented herein, linear extrapolations to the origin were made for estimating variables which were otherwise unknown and which could only be calculated from an indeterminate set of variables. Use of low order polynomial functional forms for these indeterminate grouping of variables yielded similar results to those presented herein.

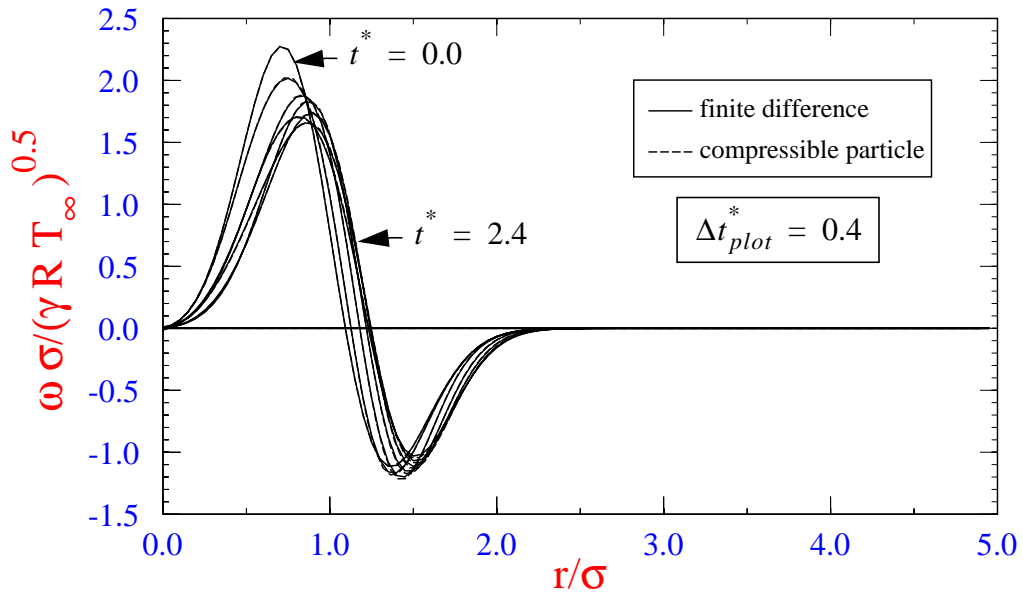


Figure 13. Vorticity Comparison for 2D Radial Flow

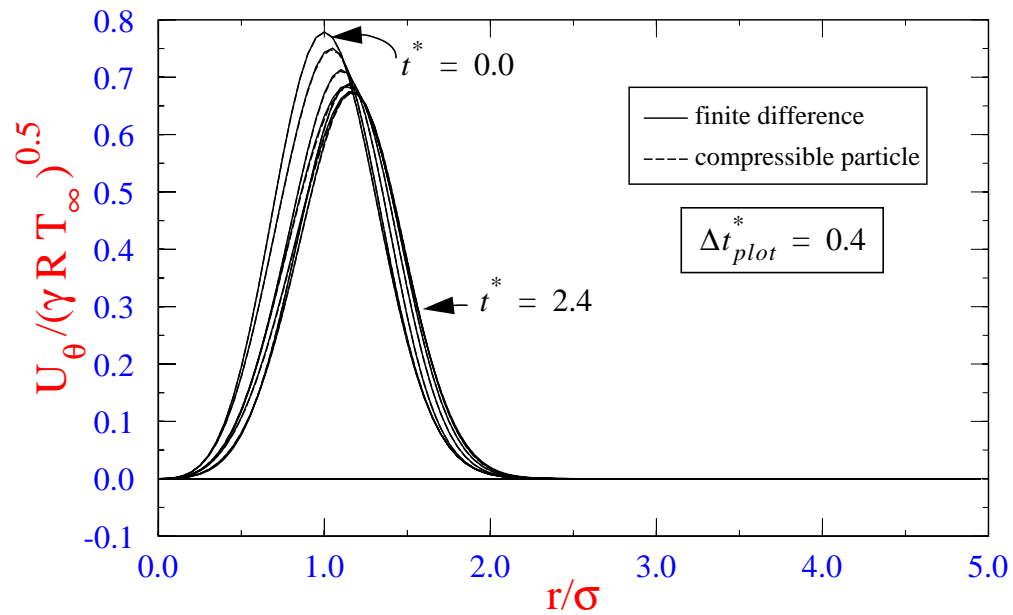


Figure 14. Tangential Velocity Comparison for 2D Radial Flow

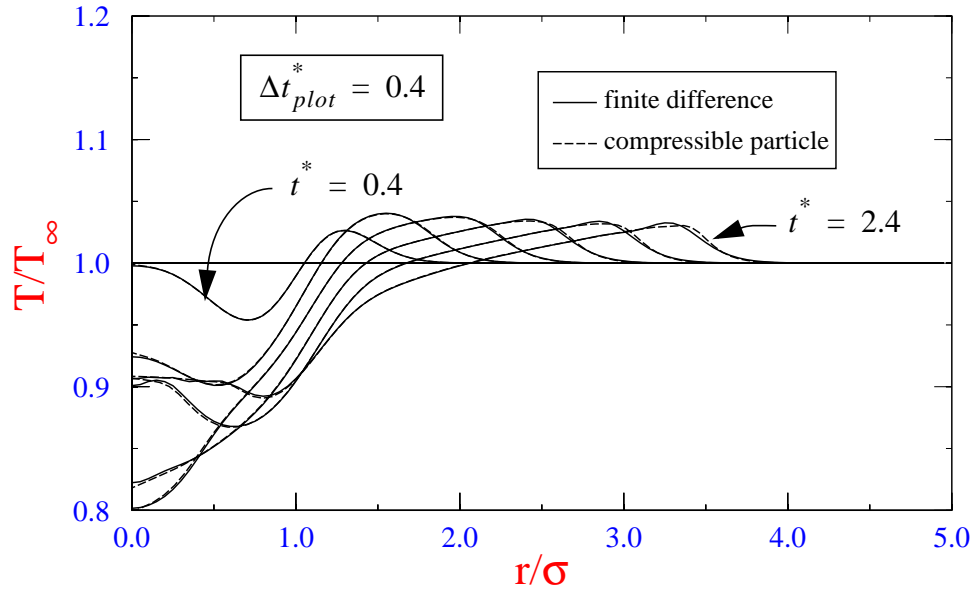


Figure 15. Temperature Comparison for 2D Radial Flow

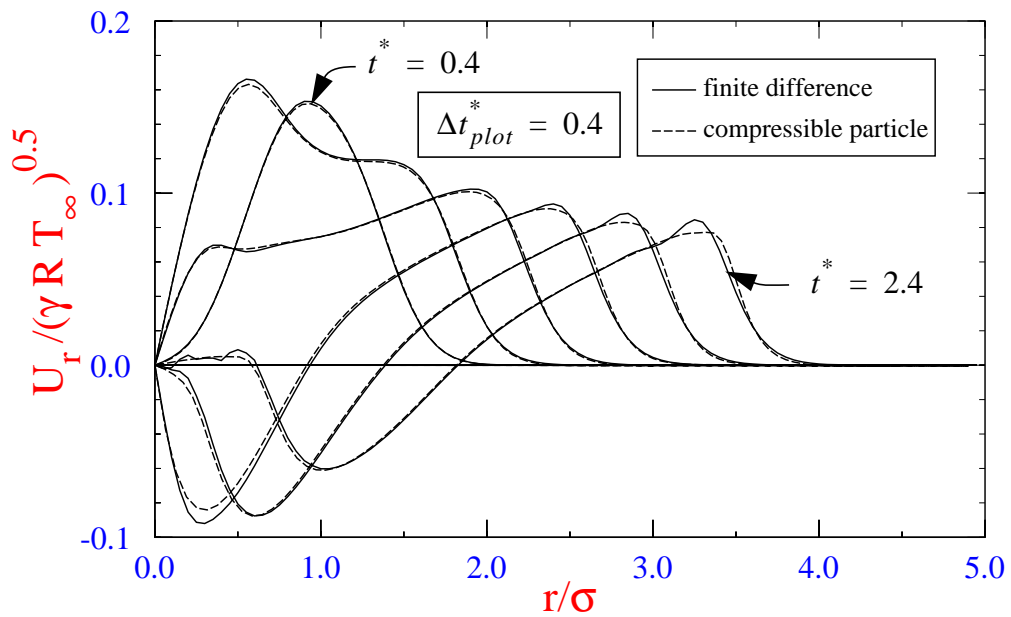


Figure 16. Radial Velocity Comparison for 2D Radial Flow

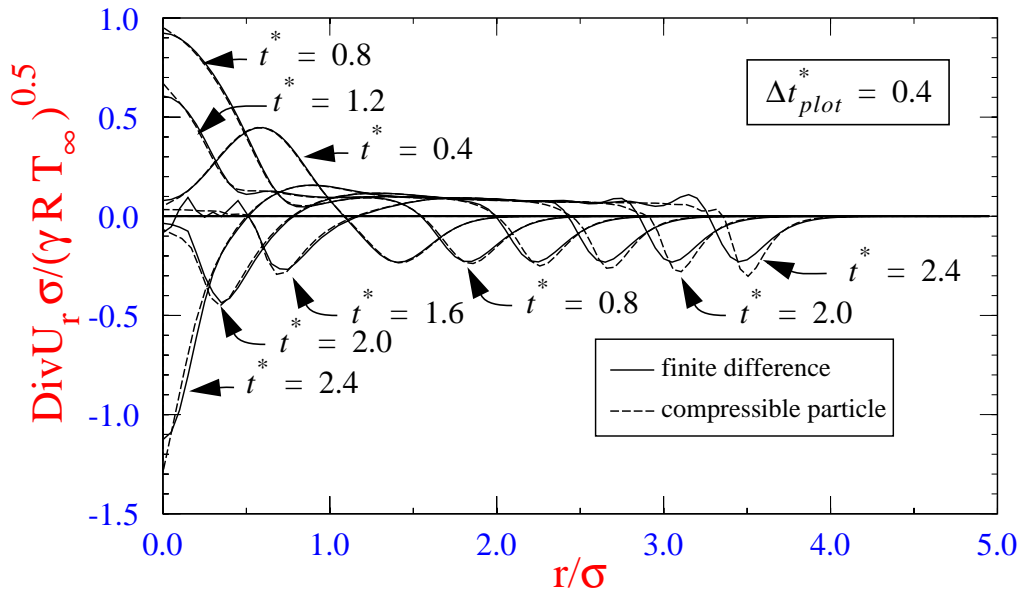


Figure 17. Divergence Comparison for 2D Radial Flow

For completeness, the particle distribution is shown in Figure 18. It is interesting to note that the particle distribution is not changed in a significant way even though the vortical disturbance contains maximum tangential velocities in the 0.7-0.8 Mach number range. Therefore, one can conclude that the effects of the sudden appearance of this vortical disturbance are primarily acoustic in nature outside of the vortical region itself.

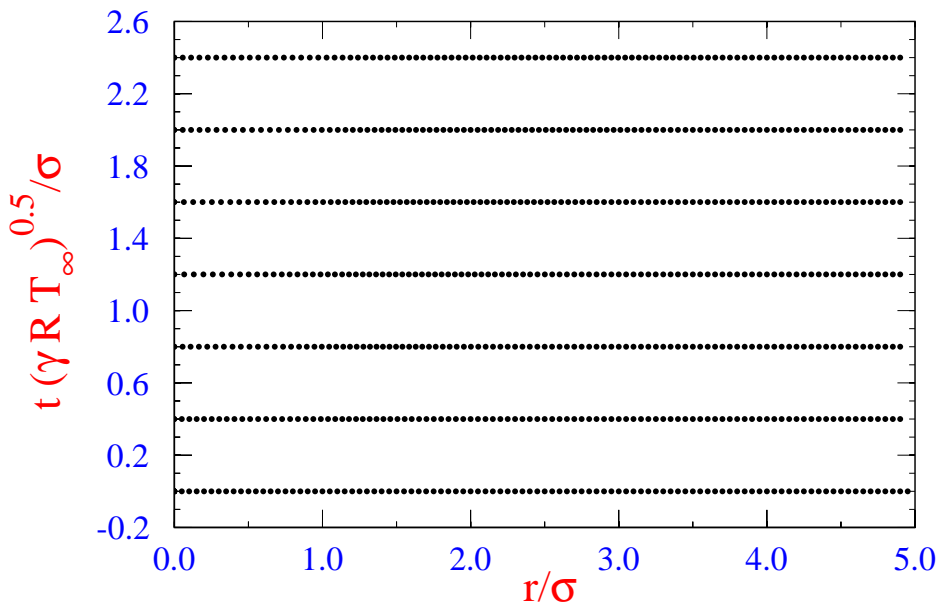


Figure 18. Compressible Particle Distribution

5 DISCUSSION

5.1 General Observations

- The Lagrangian evolution equation for the velocity divergence has been derived and examined in some detail. The right hand side of this equation may be represented in several ways, especially the term which contains the product of the deformation rate tensor and its transpose.
- The viscous terms in each of the evolution equations for divergence, vorticity, and energy are greatly simplified if one assumes constant dynamic as well as kinematic viscosity coefficients. This assumption is only valid for small variations in density.
- Results using the gridless compressible method for both an isentropic inviscid 1D spherical flow which initially has a Gaussian temperature distribution with zero velocity everywhere and an isentropic inviscid 2D radial flow which has an initial vorticity distribution with constant temperature everywhere compare favorably with results from their associated finite-difference formulations.
- The gridless compressible method possesses a natural adaptability in that particles tend to cluster in regions of high density where shock waves and sharp gradients are most likely to form.
- While divergence is generated in the flow field due to pressure disturbances, vorticity is not, so long as the flow is isentropic. For the isentropic case, vorticity is only generated at boundaries although it may be intensified by stretching, weakened by dilation, and redistributed by viscous diffusion elsewhere in the flow.

5.2 Some Questions to Answer

- In compressible flow, the discretized surface sheets carry not only values of ω but also values of δ and the thermodynamic properties p , ρ , and T . What are the appropriate values of δ and the thermodynamic properties p , ρ , and T in the nascent elements at the body surface?
- How can the formation of shocks in the flow be handled? Is shock capturing possible with a “non-conservative scheme?” Is the Lagrangian method really non conservative? For example, in inviscid flow away from boundaries and shocks, the particle circulation may be conserved. Likewise, for isentropic flow, the particle energy and mass may be conserved.
- Can core functions be developed which will mimic some of the wavelike behavior of the δ , p , ρ , and T fields? Can time splitting be used to first convect particles and then allow them to produce waves which can then be superimposed?
- Under what conditions may the divergence contributions be neglected? For example, filtering out the acoustic phenomenon in low Mach number flows or allowing acoustic signals to simply disappear at the edge of a specified domain (i.e. see Eldridge et al. [11]).
- Is it worthwhile or perhaps necessary to sub-cycle time steps in order to adapt to the different length scales associated with the diffusive, convective, and acoustic processes?

5.3 A Set of Investigations

- **Boundary Conditions:** For bounded flow or external flow over boundaries the thermodynamic properties as well as the vorticity and velocity divergence must be specified for the newly created Lagrangian particles at the boundaries. If a PSE method or the VRM is used where new particles are simply flowing over the surface, the flux from the wall into the particles must be determined. This process is well understood for vorticity but needs to be revisited for divergence and the thermodynamic properties. For instance, divergence may be generated at the wall due to an incoming pressure pulse or the temperature changed due to heat transfer from the wall into the fluid. This study should include situations where the boundary is assumed to be adiabatic as well as non-adiabatic. The pressure distribution along the wall needs to be formulated with due consideration to divergence generation at the surface.
- **Shock Capturing:** Proper treatment of shocks embedded in the flow will be necessary for simulations where the flow is no longer isentropic everywhere. The feasibility of treating the flow as being isentropic except across shocks should be investigated. Initial investigations should include a study of shock capturing methods and their applicability to the gridless Lagrangian method. As Whitham [35] points out “For shocks of weak or moderate strength, it is a reasonable approximation to neglect changes in the entropy and the Riemann invariant. With these approximations, the simple wave solution can be retained and used even when weak shocks are included.”
- **Evolution Equation Representation:** Work needs to be undertaken to develop appropriate core functions and/or use those developed by Eldridge et al. [11]. Core functions which mimic both particle and wave behavior should be investigated. In addition, core functions which are compatible with boundaries should be further developed. The method by which the Laplacian terms on the right hand side of the evolution equations are treated (i.e. PSE, VRM, diffusion velocity, etc.) should be further studied. Use of moving least squares (MLS) or some variation of the VRM should be considered for treating all of the terms on the right hand side of the evolution equations. The best form for the right hand side of the divergence evolution equation should be investigated.

5.4 Some Model Problems

- The radial flow problems should be solved using more sophisticated conservation forms of the governing equations to provide more accurate results by which to judge the gridless methods. The radial flow problems should be solved in a gridless manner by actually using the Helmholtz decomposition for obtaining the velocity field from the vorticity and divergence fields. Particles should be placed throughout the disturbed portion of the domain as opposed to the strictly radial placement used in the present study.
- One dimensional shock tube problems characterized by breaking a diaphragm separating a high and low pressure gas should be simulated using the gridless method. These results should be compared to existing exact and numerical solutions to see that the resulting shock wave, rarefaction wave, and contact discontinuity are successfully simulated.

- Free shear layer simulations such as those done by Mas-Gallic [5] should perhaps be repeated using a truly gridless method. Shear layer simulations might also include those in which heat addition is occurring such as in the work of Soteriou and Ghoniem [42].
- A number of wall-bounded flows should be examined. These can be as simple as an impulsively started infinite flat plate (a compressible version of “Stoke’s First Problem”) which requires inexpensive 1D calculations but which may be used to answer a number of fundamental modeling questions. Inviscid transonic and supersonic flows over airfoil geometries should be simulated in order to compare the gridless method against classical results. It may also be worthwhile to simulate some classical acoustic problems in which walls are involved.

(this page intentionally left blank)

6 REFERENCES

- [1] Peterson, C. W., Strickland, J. H., and Higuchi, H., "The Fluid Dynamics of Parachute Inflation," *Annual Review of Fluid Mechanics*, Vol. 28. pp. 361-387, (1996).
- [2] Strickland, J. H. and Higuchi, H., "Parachute Aerodynamics: An Assessment of Prediction Capability (1995)," *Journal of Aircraft*, Vol. 12, No. 2, pp. 241-252, March-April, (1996).
- [3] Homicz, G. F., "FY98 ESRF Effort on Gridless Methods for Compressible Flows," Sandia Laboratory Memorandum, October 14, 1998.
- [4] Nitsche, M., "Extension of the Gridless Vortex Method into the Compressible Flow Regime," Proposal for the Sandia-University Research Program, June 23, 2000.
- [5] Mas-Gallic, S., Louaked, M, and Pironneau, O., "A Particle in Cell Method for the 2-D Compressible Euler Equations," *Vortex Flows and Related Numerical Methods*, Kluwer Academic Publishers.
- [6] Mas-Gallic, S., "A Particle-In-Cell Method for the Isentropic Gas Dynamic System", in *Navier-Stokes Equations and Related Nonlinear Problems*, edited by Sequeira, A., Plenum Press, 1995.
- [7] Sod, G. A., "A Numerical Simulation of a Free Mixing Layer," *Simulation*, Vol. 54, No. 5, pp. 259-268, May 1990.
- [8] Sod, G. A., "A Compressible Vortex Method with Application to the Interaction of an Oblique Shock Wave with a Boundary Layer," *Applied Numerical Mathematics*, Vol. 8, No. 3, pp. 257-273, 1991.
- [9] Ogami, Y. and Cheer, A. Y., "Grid-Free Particle Method Applied to the Equations of Unsteady Compressible Fluid Motion," *AIAA Journal*, Vol. 31, No. 6, pp. 1155-1157, June 1993.
- [10] Ogami, Y. and Cheer, A. Y., "Simulations of Unsteady Compressible Fluid Motion by an Interactive Cored Particle Method," *SIAM Journal of Applied Mathematics*, Vol. 55, No. 5, pp. 1204-1226, October 1995.
- [11] Eldridge, J., Colonius, T., and Leonard, A., "A Vortex Particle Method for Compressible Flows," Presentation at ICTAM 2000, Chicago IL, September 1, 2000.
- [12] Greengard, L., "Fast Algorithms for Classical Physics," *Science*, Vol. 265, pp. 909-914, August 1994.
- [13] Strickland, J. H. and Baty, R. S., "An Overview of Fast Multipole Methods," *Lectures in Applied Mathematics*, Vol. 32, pp. 807-830, 1996.
- [14] Degond, P. and Mas-Gallic, S., "The weighted Particle Method for Convection-Diffusion Equations, Part 1: The case of an Isotropic Viscosity," *Math. Comput.*, Vol. 53, No. 188, pp. 485-507, 1989.
- [15] Gharakhani, A, "A Higher Order Vorticity Redistribution Method for 3-D Diffusion in Free Space," Sandia National Laboratory Report SAND2000-2505, October 2000.
- [16] Subramaniam, S., "A New Mesh-Free Vortex Method," *Ph.D. Thesis*, The Florida State University, 1996.

- [17] Curry, I. G., *Fundamental Mechanics of Fluids*, McGraw Hill, New York, 1974.
- [18] Bird, R. B., Stewart, W. E., Lightfoot, E. N., *Transport Phenomena*, John Wiley & Sons, New York, 1960.
- [19] Kempka, S. N., Glass, M. W., Strickland, J. H., and Ingber, M. S. "A Galerkin Boundary Element Method for Solving the Generalized Helmholtz Decomposition," *3rd International Workshop on Vortex Flows and Related Numerical Method*, Toulouse, France, August 24-27, 1998.
- [20] Strickland, J. H., Amos, D. E., "A Fast Solver for Systems of Axisymmetric Ring Vortices," Sandia National Laboratory Report SAND90-1925, 52 pages, September 1990. Also *AIAA Journal*, Vol. 30, No. 3, pp. 737-746, March 1992.
- [21] Carrier, J., Greengard, L., Rokhlin, V., "A Fast Adaptive Multipole Algorithm for Particle Simulations," *SIAM J. Sci. Statist. Comput.* Vol. 9, pp. 669, 1988.
- [22] Strickland, J. H. and Baty, R. S., "A Two-Dimensional Fast Solver for Arbitrary Vortex Distributions," Sandia National Laboratory Report SAND97-0880, April 1997.
- [23] Strickland, J. H. and Baty, R. S., "Modification of the Carrier, Greengard, and Rokhlin FMM for Independent Source and Target Fields," *Journal of Computational Physics*, Vol. 142, No. 1, pp. 123-128, May 1998.
- [24] Cheng, H., Greengard, L., Rokhlin, V., "A Fast Adaptive Multipole Algorithm in Three Dimensions," *Journal of Computational Physics*, Vol. 155, pp. 468-498, 1999.
- [25] Strickland, J. H., Gritz, L. A., Baty, R. S., Homicz, G. F., "Fast Multipole Solvers for Three-Dimensional Vortex and Radiation Problems," *3rd International Workshop on Vortex Flows and Related Numerical Method*, Toulouse, France, August 24-27, 1998.
- [26] Homicz, G. F. and Burns, S. P., "Parallel Performance of VIPAR," Sandia Laboratory Memo, September, 1998.
- [27] Strickland, J. H., "A Prediction Method For Unsteady Axisymmetric Flow Over Parachutes," *AIAA Journal of Aircraft*, Vol. 31, No. 3, pp. 637-643, May-June, 1994.
- [28] Wolfe, W. P., Strickland, J. H., Homicz, G. F., and Gossler, A. A. "VFLOW2D - A Vortex Based Code for Computing Flow Over Elastically Supported Tubes and Tube Arrays," Sandia National Laboratories Report SAND2000-2504, October, 2000.
- [29] Strickland, J. H., Homicz, G. F., and Gossler, A. A. Wolfe, W. P., "A 3-D Vortex Code for Parachute Flowfield Predictions: VIPAR Version 1.0, Sandia National Laboratories Report SAND2001-xxxx, March 2001.
- [30] Gharakhani, A., "A Regularized Galerkin Boundary Element Method (RGBEM) for simulating Potential Flow About Zero Thickness Bodies," Sandia National Laboratories Report SAND99-2578, October, 1999.

- [31] Ogami, Y. and Akamatsu, T., "Viscous Flow Simulation Using The Discrete Vortex Model - The Diffusion Velocity Concept," *Comp. Fluids*, Vol. 19, pp. 433-441, 1991.
- [32] Strickland, J. H., Kempka, S. N., Wolfe, W. P., "Viscous Diffusion Using the Diffusion Velocity Concept," *Vortex Flows and Related Numerical Methods II, European Series in Applied and Industrial Mathematics: Proceedings*, Vol. 1, pp. 135-151, August, 1996.
- [33] Gharakhani, A., "A Survey of Grid-Free Methods for the Simulation of 3-D Incompressible Flows in Bounded Domains," Sandia National Laboratory Report, SAND97-2256, September, 1997.
- [34] Lighthill, J., *Waves in Fluids*, Cambridge University Press, Cambridge, 1978.
- [35] Whitham, G. B., *Linear and Nonlinear Waves*, John Wiley and Sons, New York, 1977.
- [36] Sedov, L. I., *Similarity and Dimensional Methods in Mechanics*, 10th edition, CRC Press, 1993.
- [37] Marshall, J. S. and Grant, J. R., "Penetration of a Blade Into a Vortex Core: Vorticity Response and Unsteady Blade Forces," *J. Fluid Mech.*, Vol. 306, pp. 83-109, 1996.
- [38] Marshall, J. S. and Grant, J. R., "A Lagrangian Vorticity Collocation Method for Viscous, Axisymmetric Flows with and Without Swirl," *Journal of Computational Physics*, Vol. 138, pp. 302-330, 1997.
- [39] Marshall, J. S., Grant, J. R., Gossler, A. A., and Huyer, S. A., "Vorticity Transport on a Lagrangian Tetrahedral Mesh," *Journal of Computational Physics*, Vol. 161 pp. 85-113, 2000.
- [40] Wolfe, W. P., Nelson, J. M., Baty, R. S., Laguna, G. A., Mello, F. J., Hailey, C. E., and Snyder, N. T., "A Gridless Technique for Fluid/Structural Dynamic Coupling on Flexible Membranes," Sandia National Laboratory Report, SAND96-0199, January, 1996.
- [41] Anderson, J. D., *Modern Compressible Flow*, McGraw-Hill, 1982.
- [42] Soteriou, M. C. and Ghoniem, A. F., "Vorticity Dynamics of an Exothermic Spatially Developing, Forced, Reacting Shear Layer," *Proceedings of the 25th Symposium (International) on Combustion*, The Combustion Institute, pp. 1265-1272, 1995.

(this page intentionally left blank)

Distribution

- 2 Analytical Methods (2)
2133 152nd Ave.
Redmond, WA 98052
Attn: F. Dvorak
B. Maskew
- 1 Dr. P. W. Bearman
Dept. of Aeronautics
Imperial College
London, SW7 2BY
ENGLAND
- 1 Dr. J. Carrier
124 Me Pierre Termier
73000 Chambéry, FRANCE
- 1 Prof. A. J. Chorin
Department of Mathematics
University of California
Berkeley, CA 94720
- 1 Prof. Tim Colonius
Mechanical Engineering
Mail Code 104-44
California Institute of Technology
Pasadena, CA 91125
- 1 Dr. L. Cortelezzi
UCLA
Dept. of Mathematics
Los Angeles, CA 90095-1555
- 1 Dr. R. Cortez
Dept. of Mathematics
Tulane University
6823 St. Charles Ave, #424
New Orleans, LA 70118
- 1 Mr. Jeff Eldridge
017 Thomas
Mail Code 104-44
California Institute of Technology
Pasadena, CA 91125
- 1 Dr. Adrin Gharakhani
Applied Scientific Research
1800 E. Garry Ave., Suite 214
Santa Ana, CA 92705
- 1 Prof. Ahmed F. Ghoniem
Massachusetts Institute of Technology
Mechanical Engineering Dept.
Room 3-342
Cambridge, MA 02139-4307
- 1 Dr. John R. Grant
Naval Undersea Center
1176 Howell Street
Building 108, Code 8233
Newport RI 02841-1708
- 1 Prof. Leslie Greengard
Courant Institute of Math. Sciences
New York University
251 Mercer Street
New York, NY 10012
- 1 Prof. C. E. Hailey
Mech. & Aero. Eng.
Utah State University
UMC 4130
Logan, UT 84322-4130
- 1 Prof. H. Higuchi
Dept. of Mech. & Aero. Eng.
Syracuse University
Syracuse, NY 13244
- 1 Dr. Stephen Huyer
Naval Undersea Weapon Center
Hydrodynamics Branch, Code 8233
Building 1302/1
Newport, RI 02841
- 1 Dr. Vinay Kalro
Fluent, Inc.
1508 Oak Ave., #3N
Evanston, IL 60201
- 1 Prof. A. R. Karagozian
UCLA
46-147D Engr. IV
Mail Code 951597
Los Angeles, CA 90095-1597

- 1 Prof. Joseph Katz
Dept. Aerospace Eng. and Eng. Mech.
San Diego State University
San Diego, CA 92182-0183
- 1 Prof. Omar M. Knio
Dept. of Mech. Eng.
Johns Hopkins University
Baltimore, MD 21218-2686
- 1 Prof. Anthony Leonard
Graduate Aeronautics Lab.
1200 East California Blvd.
California Institute of Technology
Pasadena, CA 91125
- 1 Prof. S. Mas-Gallic
Centre de Mathematiques Appliquees
Ecole Polytechnique
91128 Palaiseau Cedex FRANCE
- 1 Dr. Jeffery S. Marshall
Iowa Institute of Hydraulic Research
University of Iowa
300 S. Riverside Drive
Iowa City, IA 52242-1585
- 1 Dr. Eckart Meiburg
Dept. of Aerospace Eng.
University of Southern California
854 W. 36th Place
Los Angeles, CA 90089-1191
- 1 Dr. D. I. Meiron
Dept. of Applied Mathematics
California Institute of Technology
Pasadena, CA 91125
- 1 Dr. M. Nitsche
Dept. of Math. & Stat.
University of New Mexico
Albuquerque, NM 87131
- 1 Prof. Y. Ogami
Dept. Mech. Eng.
Ritsumeikan University
Kusatsu 525-77, JAPAN
- 1 Prof. Ion Paraschivoiu
Dept. of Mech. Eng.
Ecole Polytechnique
CP 6079
Succursale A
Montreal H3C 3A7, CANADA
- 1 Prof. S. C. Rajan
Dept. of Aerospace Eng.
Indian Institute of Technology, Madras
Chennai, Pin 600036
Tamilnadu, India
- 1 Prof. V. Rokhlin
Department of Computer Science
Yale University
PO Box 2158
New Haven, CT 06520
- 1 Prof. P. G. Saffman
Dept. of Applied Mathematics
California Institute of Technology
Pasadena, CA 91125
- 1 Prof. William Saric
Dept of Mech. and Aerospace Eng.
Arizona State University
PO Box 876106
Tempe, AZ 85287-6106
- 1 Prof. T. Sarpkaya
Dept. Mech. Eng.
Code 69-SL
Naval Postgraduate Academy
Monterey, CA 93943
- 1 Prof. Michael S. Selig
Dept. of Aero. and Astro. Engineering
306 Talbot Lab
Urbana, IL 61801
- 1 Dr. John M. Seiner
NASA Langley Research Center
Mail Stop 165
Hampton, VA 23681-0001
- 1 Prof. J. A. Sethian
Dept. of Mathematics
University of California
Berkeley, CA 94720

- 1 Dr. David Sharpe
Department of Aeronautical Eng.
Queen Mary College
Mile End Road
London, E1 4NS
ENGLAND
- 1 Prof. Roger L. Simpson
Dept. Aerospace and Ocean Eng.
Virginia Polytechnic Institute
and State University
Blacksburg, VA 24061
- 1 Dr. Marios C. Soteriou
UTRC
411 Silver Lane
Mail Stop 129-15
East Hartford, CT 06108
- 1 Prof. John A. Strain
Department of Mathematics
University of California
Berkeley, CA 94720
- 1 Dr. S. Shankar
Quantum Corporation
MS E23
333 South Street
Shrewsbury, MA 01545
- 1 Dr. J. W. Oler
Texas Tech University
Dept. of Mech. Eng.
Lubbock, TX 79409
- 1 Prof. G. Trygvasson
Dept. Mech. Eng. and App. Mech.
University of Michigan
Ann Arbor, MI 48109-2125
- 1 Prof. O. R. Tutty
Dept. of Aero. & Astro.
University of Southampton
Highfield, Southampton, SO17 1BJ
Hampshire, United Kingdom
- 2 University of New Mexico
Dept. of Mech. Eng.
Albuquerque, NM 87106
Attn: M. S. Ingber
C. R. Truman
- 1 Dr. James Uhlman
Code 804, Bldg. 108/2
Naval Undersea Warfare Center
Newport, RI 02841-5047
- 2 U.S. Army Soldier & Biological
Chemical Command
Soldier Systems Center Natick
Kansas Street
Natick, MA 01760-5017
Attn: SSCNC-UTS (Richard Benney)
SSCNC-UTS (Keith Stein)
- 1 Prof. L. Van Dommelen
FAMU-FSU College of Engineering
2525 Pottsdamer Street, Room 229
Florida State University
Tallahassee, FL 32310-6046
- 1 Prof. C. W. Van Atta
Dept. of App. Mech. and Eng. Sci.
Mail Code 0411
University of California
La Jolla, CA 92093-0411
- 3 Washington State University (3)
Dept. Mech. & Mat'l's Eng.
Pullman, WA 99164-2920
Attn: Jacob Chung
Clayton Crowe
Tim Troutt
- 1 Prof. R. E. Wilson
Dept. Mech. Eng.
Oregon State University
Corvallis, OR 97331
- 1 Prof. G. S. Wincklemans
Center for Sys. Eng. & App. Mech.
Unité TERM, place du Levant 2,
Université Catholique de Louvain
Louvain-la-Neuve 1348
BELGIUM
- 1 Prof. Norman J. Zabusky
Dept. of Mech. and Aerospace Eng.
Rutgers University
PO Box 909
Piscataway, NJ 08855-0909

1	Dr. David Zielke	1	0835	S. N. Kempka, 9141
	Naval Research Lab, 6-4-40	1	0835	S. R. Subia, 9141
	4555 Overlook Avenue, SW	1	0835	V. L. Porter, 9142
	Washington, DC 20375	1	0835	T. E. Voth, 9117
1	0825 F. G. Blottner, 9115	1	0835	W. P. Wolfe, 9115
1	0825 W. H. Rutledge, 9115	1	0836	R. O. Griffith, 9117
1	0826 W. L. Hermina, 9113	1	0836	E. S. Hertel, 9116
1	0827 M. J. McGlaun, 9140	1	0836	C. E. Hickox, 9116
1	0828 J. A. Fernandez, 9102	1	0836	P. E. DesJardin, 9116
1	0828 K. Radloff, 9102	1	0836	C. W. Peterson, 9100
1	0828 W. L. Oberkampf, 9133	1	0836	S. R. Tieszen, 9116
1	0834 J. E. Johannes, 9114	1	0839	L. A. Gritzo, 16000
1	0834 A. C. Ratzel, 9112	1	0841	T. C. Bickel, 9100
1	0835 A. A. Gossler, 9141	1	9051	H. N. Najm, 8351
1	0835 G. F. Homicz, 9141	1	9051	L. A. Rahn, 8351
10	0835 J. H. Strickland, 9141	1	9051	W. T. Ashurst, 8351
1	0835 J. S. Peery, 9142	1	9018	Central Technical Files, 8945-1
1	0835 M. W. Glass, 9141	2	0899	Technical Library, 9616
1	0835 R. J. Cochran, 9141	1	0612	Review & Approval Desk,
1	0835 S. Burns, 9141		9612	For DOE/OSTI